Master Thesis

Modeling Energy Transfer Processes in $Gd_2O_2S:Yb^{3+}Er^{3+}$

Author:
Marieke Castelijns

Supervisors:
Dr. F.T. Rabouw
Prof. dr. A. Meijerink

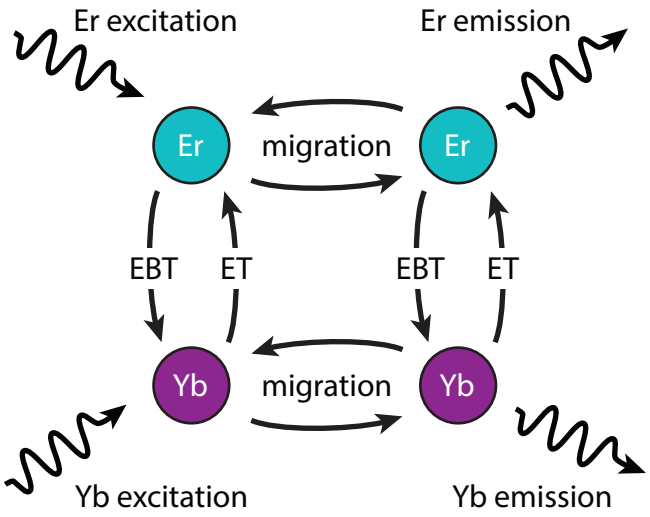

Condensed Matter and Interfaces
Debye Institute for Natomaterials Science
Utrecht University

April, 2016

Abstract

In literature, several models have been developed to describe energy transfer processes between luminescent ions. These models however sometimes fail to accurately describe real systems because they make certain assumptions e.g. random distributions of luminescent ions or fast migration, which are not always true. In this work, a model was developed that includes all the microscopic properties of the luminescent crystal and can accurately describe the behavior of its luminescent ions. The luminescent phosphor investigated in this thesis is the Yb^{3+}/Er^{3+} couple embedded in a Gd_2O_2S host, which is well known for its upconverting ability. Experimental photoluminescence decay data of high quality samples were fitted to the model to obtain parameters for the different processes taking place in the crystal. The following parameters were obtained: $\gamma_{Yb} = 3.45$ ms^{-1}, $\gamma_{Er} = 0.51$ ms^{-1}, energy transfer strength $=$ 3.71 ms^{-1}nm^6, and energy back transfer strength $= 3.64$ ms^{-1}nm^6. These parameters were used in Monte Carlo simulations to accurately model the behavior of the luminescent ions in the crystal for different concentrations.

Contents

1 Introduction

Luminescent phosphors are an important class of materials that are comprehensively used for lighting, displays [1], and bio-imaging [2]. The mechanism used to describe energy transfer between two light sensitive centers in such materials is Förster resonance energy transfer (FRET). In this transfer process, the luminescent center that becomes excited is referred to as the donor ion and the luminescent center to which the energy is transferred is called the acceptor ion. The efficiency of this energy transfer (ET) strongly depends on the distance between the donor and acceptor [3].

A popular luminescent material containing donor and acceptor ions is a crystal that is co-doped with Yb^{3+} and Er^{3+} ions. The crystal has the ability to convert photons with a low energy to photons with a higher energy. This process is called upconversion (UC). The Yb^{3+}/Er^{3+} is known as one of the most efficient near-IR to visible upconversion couple [4] and attracts interest because of its potential application in optical waveguide amplifiers [5], sensitive bio-probes [6], and emissive displays [7]. Simultaneous green and red emission from the Er^{3+} ions can be obtained while exciting in the IR. The Er^{3+} ions have a low-absorption cross-section [8], which means that they cannot be excited efficiently. This is why the Yb^{3+} ions are introduced to the crystal. Yb^{3+} ions get excited more easily since their absorption cross-section at 980 nm is about an order of magnitude larger than that of Er^{3+} [9]. In addition, Yb^{3+} is the ideal candidate because of its broad absorption band, and the large overlap between Yb^{3+} and Er^{3+} absorption. These properties allow for resonant energy transfer from Yb^{3+} to Er^{3+}. In figure 1, the two energy transfer steps that lead to visible emission are depicted. The first ET step excites the Er^{3+} ion to the $^4I_{11/2}$ level and the second ET step excites the Er^{3+} ion to the $^4F_{7/2}$ level. Visible emission can be detected from the $^2H_{11/2}$ and $^4S_{3/2}$ levels (green) and the $^4F_{9/2}$ level (red).

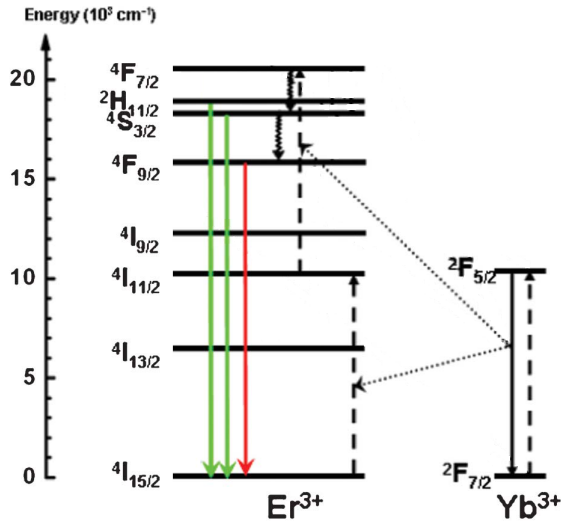

Figure 1: Schematic representation of the UC process in a Yb^{3+}/Er^{3+} system. The first energy transfer from Yb^{3+} to Er^{3+} brings the Er^{3+} ions to the $^4I_{11/2}$ level. The second energy transfer step brings the Er^{3+} ions to the $^4F_{7/2}$ level. Visible emission can be detected from the $^2H_{11/2}$ and $^4S_{3/2}$ levels (green arrows) and the $^4F_{9/2}$ level (red arrow). The figure was adapted from the work of Song et al. [10]

The efficiency of upconversion is greatly affected by the transfer probability from donor to acceptor, the transfer probability from acceptor back to donor, and the migration of energy over donors and acceptors. To improve the efficiency of upconversion, more knowledge of these processes is crucial. In the past, several models have been developed to describe these processes. The Inokuti-Hirayama model for instance describes the energy transfer from donors

to acceptors [11]. This model however does not take migration into account. In 1967, Yokota and Tanimoto tried to approximate donor-to-donor migration by regarding it as a diffusion process [12]. This implies that all the luminescent ions are randomly distributed and therefore all donor-donor distances are possible. The same holds for the model of Burshtein [13], who described the donor-donor migration as a hopping mechanism instead of a diffusion process. In a crystalline environment however, the luminescent ions are arranged in a highly ordered structure so they can only be at specific distances from each other. Furthermore, these models only describe ET processes to ions in their ground states, so they cannot model upconversion processes. To describe UC, Grant developed an average rate equation model [14]. He uses a system of coupled differential equations to describe the population of all the energy levels as a function of time. The equations can include nonlinear terms in the populations and hence this theory can model upconversion [15]. However, one major drawback is that it assumes that energy migration among the ions is fast. As a consequence, an excitation senses an average environment. This however may not be true. Especially at low concentrations, migration can be limited.

This work will develop a model that includes all the microscopic properties of the luminescent crystal and can accurately describe the behavior of its luminescent ions. Experimental photoluminescence decay data of high quality samples will be fitted to the model to obtain parameters for the different processes taking place in the crystal. These parameters will be used in Monte Carlo simulations to accurately predict the behavior of luminescent ions in a crystal for different concentrations. By altering the different input parameters, the model should be able to describe other systems in which energy transfer processes take place.

2 Theory

2.1 Lanthanides

The luminescent ions investigated in this thesis belong to the lanthanides. Lanthanides are the elements with an atomic number from 57 (La) to 71 (Lu). In this series, the $4f$ orbitals are filled up. The partly filled $4f$ shell gives rise to unique luminescent properties that make lanthanides promising for multiple applications such as biological assays and medical imaging [16]. The lanthanides are most stable in their trivalent from (Ln^{3+}). They then have an electron configuration of [Xe]$4f^n$, with n ranging from 0 to 14. The number of configurations for n electrons divided over fourteen $4f$ orbitals is large, namely $\binom{14}{n}$. Since the $4f$ orbitals have different shapes, various distributions of electrons will give rise to different electrostatic interactions, resulting in many different energy levels [17]. All these energy levels cause lanthanide ions to have many transitions in the $4f$ shell which are in the UV-VIS-IR region. That is why they are commonly used in upconversion experiments [18].

The interactions responsible for the biggest splitting in energy are Coulomb repulsion and spin-orbit coupling [19]. The latter describes the interaction between an electron's spin and the magnetic field generated by the electron's orbit around the nucleus. All the $4f^n$ energy levels are characterized by term symbols, $^{2S+1}L_J$ which consist of the quantum numbers S, L and J [20]. Here, $S = \sum m_s$ and $L = \sum m_l$, which are the vector sum of the spin and orbital angular momentum of the electronic state. Instead of using a number, L is represented by letters, similar to subshell designations. Energy states for which L = 0,1,2,3,4... are known as S, P, D, F, G... terms. To properly account for spin-orbit coupling, the quantum number J is introduced, which has possible values of $|L - S|, ..., |L + S|$ [21]. An example of a term symbol is $^2F_{7/2}$ for the ground state of an Yb^{3+} ion ($S = \frac{1}{2}$, L = 3, $J = \frac{7}{2}$).

Another interesting property of the lanthanide ions is that the $5s$ and $5p$ shell shield the inner $4f$ shell. Because of this, the electronic transitions are almost independent of the crystal field effects caused by the surrounding host material [22]. This led to the opportunity to make a general energy level diagram of the $4f^n$ energy levels in lanthanide ions. Figure 2 shows this diagram, known as the Dieke diagram. This diagram can be very valuable for predicting the optical properties of lanthanide doped materials. For different host materials, the energies of the levels can shift slightly or split in the crystal field, but the changes in energy are within the width of the horizontal bars in the Dieke diagram. Another consequence of the shielding of the $4f$ electrons is that f-f transitions hardly have any influence on the strength of chemical bonding between the lanthanide ion and surrounding ligands. As a result, the transitions have narrow absorption and emission lines and negligible Stokes shifts [23]. An additional characteristic of the f-f transitions is that they have low molar absorption coefficients. This can be ascribed to the fact that all the $4f$ states have odd parity ($l = 3$). Hence all $4f^n \rightarrow 4f^n$ transitions are parity forbidden for a free ion. The transitions become partially allowed when the lanthanide ions are embedded in a crystal system, through admixture of opposite-parity wavefunctions like $5d$ into the $4f$ wavefunctions [24]. So although the crystal field of the host material hardly influences the energy levels of the $4f$ states, its presence is essential for f-f transitions to occur.

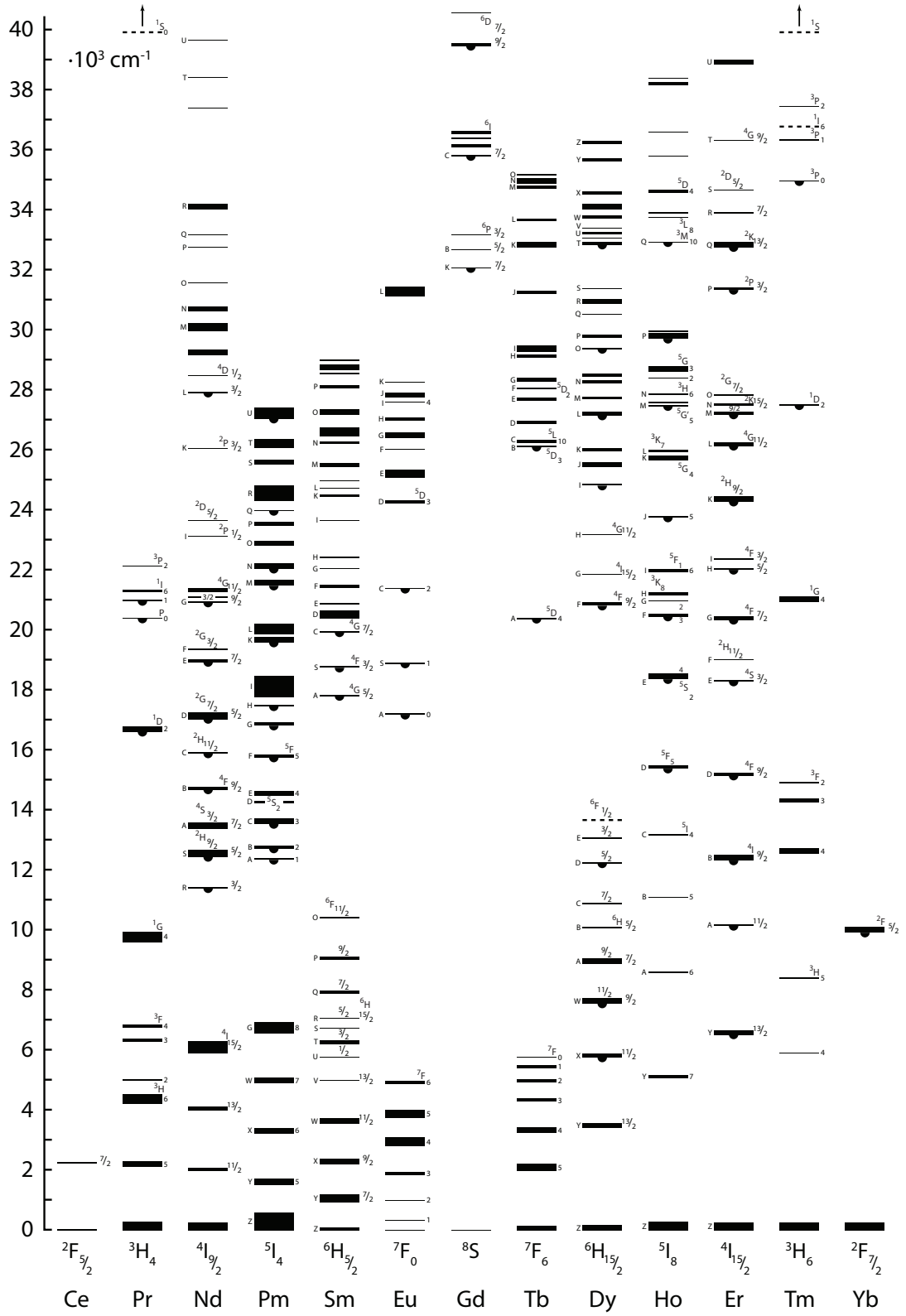

Figure 2: Dieke diagram depicting the energy levels of the $4f^n$ configurations of trivalent lanthanide ions. The width of the horizontal lines reflect the maximum splitting of the corresponding level in a crystal field. Figure copied from the work of Mathijs de Jong.

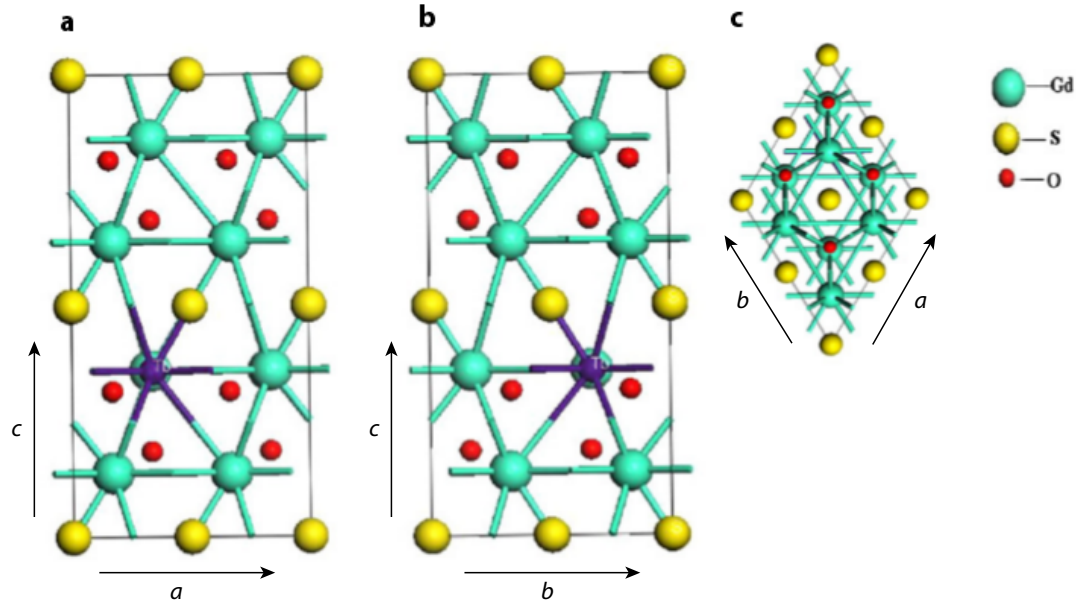

Figure 3: A 2x2x2 doped super-cell with the crystal structure of Gd_2O_2S from three different views. (**a**) The $(1, 0, 0)$ plane, (**b**) the $(0, 1, 0)$ plane and (**c**) the $(0, 0, 1)$ plane. The purple sites represent dopant ions. Figure copied from F. Wang et. al. [27]

2.2 The Crystal Host Lattice

Before making the crystal system, we have to choose the host in which we embed the desired lanthanide ions. The host material is of importance because it influences the energy transfer processes for two reasons. The first reason is multi-phonon relaxation due to the lattice vibrations. Every crystal host has its own typical vibrations and corresponding phonon energy. Via coupling, phonons provide a non-radiative channel between energy levels that competes with the radiative transitions. This non-radiative energy loss is an undesired process. To decrease multi-phonon relaxation between closely spaced energy levels, a host with low phonon energy is preferred. As a rule of thumb it holds that when energy levels are separated by less than five times the maximum phonon energy of the host, non-radiative multiphonon relaxation will be dominant [18]. For energy differences that are larger than five times the phonon energy, radiative decay will dominate. $NaYF_4$, Gd_2O_2S and BiOCl are examples of hosts which have low phonon energies ($\pm$ 450 cm^{-1}) [25]. In this research, Gd_2O_2S will be used as a host because it is available to us with a very high quality.

The second reason that the host influences the energy processes is because it only allows for specific distances between dopant ions. Every host has a specific symmetry and its own typical unit cell size. The possible distances between two cation sites are therefore characteristic for the host. Since the dopant ions occupy the cation site, the distances between them is also dependent on the host. In section 2.4.2 of this thesis, we will see how the energy transfer exactly depends on the distance between ions. Gd_2O_2S crystallizes in the $P\bar{3}m1$ space group, similar to other rare earth oxysulfides in the hexagonal system [26]. If Gd_2O_2S is doped with different lanthanides, these lanthanides will occupy the Gd-site in the crystal. Figure 3 shows three different views of a 2x2x2 doped super-cell. According to Wyckoff [26], a single unit cell has the length of $a = b = 0.38514$ nm and $c = 0.6670$ nm, and the Gd-ions are positioned at two sites within the unit cell: $(\frac{1}{3}, \frac{2}{3}, 0.245)$ and $(\frac{2}{3}, \frac{1}{3}, 0.755)$.

2.3 Förster Resonance Energy Transfer

In many doped crystals an interplay between different luminescent ions is used, which enables the independent tuning of absorption and emission [28]. In such crystals, energy transfer plays a crucial role. To describe the energy transfer between two luminescent ions, the mechanism of Förster resonance energy transfer is applicable [29]. When a donor is in the excited state, it can transfer its energy to an acceptor through non-radiative dipole-dipole coupling. The efficiency of this energy transfer depends on spectral overlap between donor emission and acceptor absorption, the distance between donor and acceptor, and the relative orientation of their dipole moments. The transfer rate γ_{ET} is given as:

$$\gamma_{\mathrm{ET}} = \frac{1}{\tau_{\mathrm{rad}}} \left(\frac{r_0}{r} \right)^6 \tag{2.1}$$

with τ_{rad} the radiative lifetime of the donor excited state and r_0 the critical distance from donor to acceptor, for which the energy transfer rate equals the decay rate of the donor. The rate of energy transfer is inversely proportional to the sixth power of the distance between a donor and acceptor. Because of this strong dependence on the distance, Förster resonant energy transfer is very efficient when a donor-acceptor pair is close together but very rapidly becomes unlikely when the distance between a donor-acceptor pair is increased.

The Förster resonant energy transfer rate can also be written in terms of $c_{\mathrm{don}\to\mathrm{acc}}$, the energy transfer strength:

$$\gamma_{\mathrm{ET}} = \frac{c_{\mathrm{don}\to\mathrm{acc}}}{r^6} \tag{2.2}$$

To calculate the critical distance r_0 between a donor and acceptor, we can equal the radiative decay rate of the donors to the energy transfer rate.

$$\gamma_{\mathrm{rad}} = \gamma_{\mathrm{ET}} \left(r = r_0 \right) = \frac{c_{\mathrm{don}\to\mathrm{acc}}}{r_0^6} \tag{2.3}$$

Rearranging gives us the expression for the Förster radius:

$$r_0 = \sqrt[6]{\frac{c_{\mathrm{don}\to\mathrm{acc}}}{\gamma_{\mathrm{rad}}}} \tag{2.4}$$

The more efficient the energy transfer process is, the larger the Förster radius will be.

Although energy transfer may be a desired process for spectral conversion, it can in practice also lead to undesired effects. At high concentrations, the probability of energy transfer increases and the energy can efficiently migrate from one luminescent centre to another [30]. With this, the probability that the energy reaches a quenching site also increases drastically. A quenching site can be a vacancy or impurity in the crystal lattice. Once the energy reaches a quenching site, the energy is lost non-radiatively and this results in a drop of the luminescence intensity and lifetime.

2.4 Modeling Energy Transfer Processes

When studying luminescent processes, emission and excitation spectra can be measured to locate the positions of the different energy levels. Additional information can be obtained by photoluminescence decay measurements. For these measurements, short laser pulses bring luminescent centers in their excited state. Multiple processes can take place that bring the luminescent ions back to their ground state. These processes all have their own rate constant on which the probability that the decay process occurs depends. At least one of these processes must be radiative for a decay curve to be measurable. In a decay curve, the emission intensity is plotted against time. The decrease in emission intensity over time depends on the total rate: the sum of all the rate constants. The total rate can be extracted from a decay curve. The total

rate can be used to calculate the lifetime of the excited state, which is equal to the inverse of the total rate ($\tau = \frac{1}{\gamma_{\text{tot}}}$). The shape of the decay curve and the magnitude of the lifetime depend on the radiative and non-radiative processes that take place in the crystal. In the following sections, we will first discuss the radiative decay of the donor ions. Secondly, we will describe how the decay of the donors is affected by energy transfer when acceptor ions are introduced to the crystal. Thirdly, the effect of migration will be described. Lastly, we will look at systems in which energy back transfer can occur.

2.4.1 Radiative decay of the donor ions

The most simple case is a bulk crystal that contains donor ions only. After excitation, the only processes that take place influencing the decay curve are radiative and nonradiative decay to the ground state. The number of excited ions after a laser pulse will decay exponentially by:

$$N(t) = N(0)e^{-\Gamma t} \tag{2.5}$$

with Γ the intrinsic decay rate of the donor ions, which is composed of a radiative rate γ_{rad}, and a non-radiative rate γ_{nonrad}. It is best to take a sample with a low concentration of donor ions when measuring the intrinsic lifetime, because at high concentrations, concentration quenching becomes more likely and this can decrease the excited state lifetime as discussed in section 2.3.

When measuring decay curves, we have to take into account that in the case of a large density of absorbing centers e.g. due to a dense packing, a photon emitted by a luminescent ion can be reabsorbed by another ion in the system. This process is called reabsorption and especially happens at high concentrations of luminescent ions. A reabsorbed photon has to be emitted a second time before it can be detected, and this takes time. This delay in time will result in a measured lifetime that is longer than the intrinsic lifetime. The crystal powders can be diluted with $BaSO_4$ to stop reabsorption from happening. $BaSO_4$ does not absorb any photons so the only result of its presence is a separation of the microcrystals in space. Because of this, an emitted photon has less chance of encountering another absorption center on its path to the detector.

2.4.2 Energy transfer to acceptor ions

The situation becomes more complex when acceptor ions are introduced to the crystal. In this system the donor ions have an extra pathway to get back to their ground state, namely via energy transfer. If we assume for simplicity that the intrinsic rate of the donors is purely radiative, the total rate is now the sum of the radiative rate and the energy transfer rate.

$$\Gamma = \gamma_{\text{rad}} + \gamma_{\text{ET}} \tag{2.6}$$

The radiative rate is the same for every donor ion, as the acceptor ions do not have an influence on this. As discussed in section 2.3, the rate of energy transfer strongly depends on the distance between a donor-acceptor pair. If we look at a system with a low concentration of donor ions, the energy cannot efficiently migrate over the donor ions and therefore every donor has a specific FRET-rate which depends on the environment of the donor. More specifically, the FRET-rate depends on the number of nearby acceptors and the distance from them. Since the radiative rate is the same for all donors, the luminescence intensity of donor emission is proportional to $N(t)$, the number of donor ions still in the excited state at time t after the pulsed excitation: $I(t) \propto \gamma_{\text{rad}} N(t)$. $N(t)$ decays non-exponentially since the ensemble contains many donors with a different environment and therefore a different γ_{ET}. Because of the crystalline nature of the host material, acceptor ions can only be situated at particular distances from the donor ions. For our convenience, we can group the cation sites in shells, so that all sites within the same shell have the same distance towards a donor ion. The environment of a single donor can then be fully described by an array $\mathbf{m}$, giving for each shell i, the number

m_i of sites actually occupied by an acceptor, and the distance r_i to the acceptor. Each nearby acceptor adds $\frac{c}{r^6}$ to the FRET rate, with c the energy transfer strength and r the distance from the donor. The total decay rate for a donor with environment $\mathbf{m}$ is then given by:

$$\Gamma(\mathbf{m}) = \gamma_{\text{rad}} + c \sum_{i}^{\text{shells}} \frac{m_i}{r_i^6} \tag{2.7}$$

To calculate the probability P of finding an environment $\mathbf{m}$, two things have to be taken into account. The first is that the acceptor occupation of shell i and $j \neq i$ are not correlated. The second is that for each shell, the probability to find m_i acceptors is binomially distributed, depending on the number of cation sites in the shell n_i and the ensemble averaged fraction ϕ of cation sites occupied by an acceptor.

$$P(\mathbf{m}) = \prod_{i}^{\text{shells}} p(m_i) \tag{2.8}$$

$$p(m_i) = \binom{n_i}{m_i} \phi^{m_i} (1-\phi)^{n_i - m_i} \tag{2.9}$$

We can write an expression for $N(t)$ as a sum over the decays of excited donors of different environments, with the appropriate weights:

$$N(t) = N(0) \sum_{\mathbf{m}} P(\mathbf{m}) e^{\Gamma(\mathbf{m})t}, \tag{2.10}$$

where the summation runs over the possible values of m_i for all shells i. Combining equation 2.10 with equation 2.7 and 2.8 yields after some algebra:

$$N(t) = N(0) e^{-\gamma_{\text{rad}} t} \prod_{i}^{\text{shells}} \sum_{m_i=0}^{n_i} p(m_i) e^{-c m_i t / r_i^6}. \tag{2.11}$$

Using equation 2.9 and the binomial theorem $(A+B)^n = \sum_{k=0}^{n} \binom{n}{k} A^k B^{n-k}$ we arrive at

$$N(t) = N(0) e^{-\gamma_{\text{rad}} t} \prod_{i}^{\text{shells}} (1 - \phi + \phi e^{-ct/r_i^6})^{n_i}, \tag{2.12}$$

where the terms in the product represent the effect of each shell on the emission intensity. Since c, t and r all have to be positive, the exponent can never become greater than 1. If $t \neq 0$, the exponent can only be smaller than 1. As a conclusion we can say that as we predicted, the possibility of energy transfer makes the decay of the donor ions faster. For a larger value of the energy transfer strength c, e^{-ct/r^6} becomes smaller and therefore the decay of the donor ions becomes faster. The same goes for a larger value of the concentration of acceptor ions ϕ. This is what we expect since the more energy is transferred to acceptors, the faster the population of excited donor shrinks, so the faster the decay will be. Furthermore, we can tell from this equation that for a large distance r, e^{-ct/r_i^6} approaches 1. This means that shells far away hardly affect the decay curve. This is a direct effect of the short range of FRET.

2.4.3 Energy migration over donor ions

When there is a high concentration of donor ions present in the crystal system, the luminescent ions are close together and because of this, migration will start to play a role. Because of this migration, finding an expression for $N(t)$ generally becomes too complex to solve analytically. However, for a system where the donor-to-donor migration is very fast compared to radiative decay and energy transfer, an expression can still be found. In this case, the excitation energy

can travel very fast over many donor ions and therefore senses an average environment of acceptor ions. To calculate the average energy transfer rate, we have to sum over the rate for all lattice sites and multiply by ϕ, the acceptor concentration:

$$\langle \gamma_{\mathrm{ET}} \rangle = \phi \sum_{i}^{\text{shells}} \frac{c n_i}{r_i^6}. \tag{2.13}$$

In this case, a further increase in the donor concentration will have no influence on the decay rate. The rate of the donor ions can now be describes as:

$$\Gamma = \gamma_{\mathrm{rad}} + \phi \sum_{i}^{\text{shells}} \frac{c n_i}{r_i^6}. \tag{2.14}$$

In the intermediate region where the donor-donor migration strength is comparable to the energy transfer strength, it can be helpful to turn to computer simulations.

Monte Carlo simulations come in helpful to model our crystal system. Monte Carlo simulations are based on repeated random sampling to obtain numerical results. A more elaborate description of Monte Carlo simulations and its parameters will be given in section 2.5. Our approach is to simulate a crystal host system with randomly distributed dopant ions. If the exact distribution is known, the donor-donor and donor-acceptor distances can be calculated. An analytic expression can be obtained for $n(t)$, the donor population. If we sample over many crystal systems, the macroscopic behavior of the donor ions can be described which includes the microscopic properties. The method used to derive an expression for $n(t)$ that will be described here, was developed by F.T. Rabouw and J. Haitjema [31].

In a crystal system that contains a high concentration of donor ions as well as acceptor ions, an excitation laser pulse instantaneously excites a subset of the donor ions. For each ion, a differential equation can be derived to describe its behavior over time. The population of donor i evolves as

$$\frac{\mathrm{d}n_i}{\mathrm{d}t} = -\gamma_{\mathrm{rad}} n_i + \sum_{j \neq i}^{\text{don.}} M_{i \leftrightarrow j}[(1-n_i)n_j - n_i(1-n_j)] - \sum_{k}^{\text{acc.}} T_{i \to k} n_i, \tag{2.15}$$

with n_i the probability that donor i is in the excited state, γ_{rad} the radiative rate of the donor ions, $M_{i \leftrightarrow j}$ the donor to donor energy migration rate and $T_{i \to k}$ the donor to acceptor energy transfer rate. The first and third term in the equation are both negative since radiative decay and energy transfer to acceptors both give a decrease in the excited state population. The second term in the equation describes both energy transfer from ion i to j (negative) and the reverse process of energy migration from j to i (positive). We assume equal rates for these migrations. The values of $M_{i \leftrightarrow j}$ and $T_{i \to k}$ strongly depend on the distances between the ions involved. We can rewrite the equation above to

$$\frac{\mathrm{d}}{\mathrm{d}t}\mathbf{n} = \frac{\mathrm{d}}{\mathrm{d}t}\begin{pmatrix} n_1 \\ n_2 \\ n_3 \end{pmatrix} = \begin{pmatrix} -\Gamma_1 & M_{1\leftrightarrow 2} & M_{1\leftrightarrow 3} & \cdots \\ M_{2\leftrightarrow 1} & -\Gamma_2 & M_{2\leftrightarrow 3} & \cdots \\ M_{3\leftrightarrow 1} & M_{3\leftrightarrow 2} & -\Gamma_3 & \cdots \\ \vdots & \vdots & \vdots & \ddots \end{pmatrix} \begin{pmatrix} n_1 \\ n_2 \\ n_3 \end{pmatrix} = \mathbf{A}\mathbf{n}, \tag{2.16}$$

with

$$\Gamma_i = \gamma_{\mathrm{rad}} + \sum_{j \neq i}^{\text{don.}} M_{i \leftrightarrow j} + \sum_{k}^{\text{acc.}} T_{i \to k} \tag{2.17}$$

the total decay rate of donor ion i. The general solution of this system of rate equations is

$$\mathbf{n}(t) = \sum_i c_i \mathbf{v}_i e^{-\gamma_i t}, \tag{2.18}$$

where γ_i and $\mathbf{v}_i$ are the eigenvalues and corresponding eigenvectors of rate matrix $\mathbf{A}$. The coefficients c_i are determined by the initial distribution of excitation energy $\mathbf{n}(0)$:

$$\mathbf{c} = \mathbf{V}^{-1}\mathbf{n}(0) \tag{2.19}$$

with $\mathbf{V} = (\mathbf{v}_1\ \mathbf{v}_2\ \mathbf{v}_3\ \cdots)$. Following the excitation of a single donor k, the population evolution is described by equation 2.18 with $c_i = c_i^{(k)} = (V^{-1})_{ki}$.

For a particular excitation distribution $\mathbf{n}(0)$, the light intensity recorded after time t is proportional to the total population of excited donors:

$$I(t) \propto \sum_j^{\text{don.}} n_j(t) = \sum_i \left(c_i \sum_j^{\text{don.}} V_{ij} e^{-} \gamma_i t \right) \tag{2.20}$$

If we assume that the excitation power is low, so there is no saturation of acceptor ions, the experimental photoluminescence decay curve results from averaging equation 2.20 over all possible single-donor excitations k:

$$\begin{aligned} I(t) \propto \sum_k^{\text{don.}} \sum_j^{\text{don.}} n_j^{(k)}(t) &= \sum_i \left(\sum_k^{\text{don.}} c_i^{(k)} \sum_j^{\text{don.}} V_{ij} e^{-\gamma_i t} \right) \\ &= \sum_i \left(\sum_k^{\text{don.}} (V^{-1})_{ki} \right) \left(\sum_j^{\text{don.}} V_{ij} \right) e^{-\gamma_i t} \end{aligned} \tag{2.21}$$

where $n_j^{(k)}(t)$ denotes the probability that donor ion j is excited after time t following initial excitation in donor ion k. We see that the decay curve contains rate components γ_i with weights $\left(\sum_k^{\text{don.}} (V^{-1})_{ki}\right) \left(\sum_j^{\text{don.}} V_{ij}\right)$.

2.4.4 Energy back transfer

Thus far we described the influence of energy transfer and energy migration on the decay of the donor ions. For some systems, these two processes are sufficient to describe the decay of the donors. For other systems however, an extra energy transfer process should be taken into account: energy back transfer (EBT).

Not all donor-acceptor systems can be treated equally. If we for example look at $LaPO_4$ nanocrystals codoped with Ce^{3+} and Tb^{3+}, the acceptor ion has multiple energy levels that lie closely together (see figure 4). As a consequence, some of the transferred energy is quickly lost via relaxation until a metastable state is reached. From this metastable state, radiative decay can take place. In this case, the energy transfer is accompanied by a loss in energy. It is unlikely that the acceptor ion can transfer energy back to the donor ion, because extra energy will be needed to account for the initial loss. However in some systems, including our Yb^{3+}/Er^{3+}-system, the energy levels of the donor and acceptor ion have a big spectral overlap. If this is the case, energy transfer from the acceptor back to the donor ion is a very plausible process. This is called energy back transfer. Most of the time, this is an undesired process because we would like the energy to be located on the acceptor and not on the donor ions.

We will now describe the influence of the energy back transfer on the rate of the donor and acceptor ions. If we consider a system that contains a high concentration of donor and acceptor ions in which radiative decay, energy transfer, energy migration and energy back transfer can take place, the excited state dynamics would be as follows.

$$\begin{aligned} \frac{\mathrm{d}}{\mathrm{d}t} x_{\text{don}} X_{\text{don}} = &-k_{\text{don}} x_{\text{don}} X_{\text{don}} - W_{\text{ET}} x_{\text{don}} X_{\text{don}} (1 - x_{\text{acc}}) X_{\text{acc}} \\ &+ W_{\text{BT}} x_{\text{acc}} X_{\text{acc}} (1 - x_{\text{don}}) X_{\text{don}} \end{aligned} \tag{2.22}$$

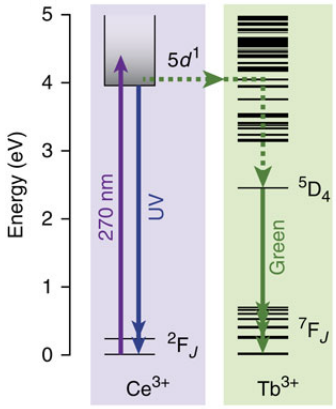

Figure 4: The energy level diagrams of Ce^{3+} and Tb^{3+} in $LaPO_4$ nanocrystals. Absorption of a UV photon (purple) brings Ce^{3+} in the excited state. Ce^{3+} can transfer its energy to a Tb^{3+} acceptor (dashed green arrow). Tb^{3+} rapidly relaxes to the $^5D_4$ metastable state, followed by radiative decay to the ^7F_J ground state under the emission of a green photon (solid green arrows). Because of the rapid relaxation, energy back transfer becomes very unlikely. Figure copied from the work of F.T. Rabouw et al. [32]

$$\frac{\mathrm{d}}{\mathrm{d}t}x_{\mathrm{acc}}X_{\mathrm{acc}} = -k_{\mathrm{acc}}x_{\mathrm{acc}}X_{\mathrm{acc}} + W_{\mathrm{ET}}x_{\mathrm{don}}X_{\mathrm{don}}(1-x_{\mathrm{acc}})X_{\mathrm{acc}} - W_{\mathrm{BT}}x_{\mathrm{acc}}X_{\mathrm{acc}}(1-x_{\mathrm{don}})X_{\mathrm{don}} \tag{2.23}$$

with X_{don} and X_{acc} the total number of donor and acceptor ions, x_{don} and x_{acc} the fraction of ions in the excited state and W_{ET} and W_{BT} the energy transfer and energy back transfer parameters. W_{ET} (W_{BT}) is the total energy (back) transfer rate that accounts for all the possible energy (back) transfers in the crystal. We can obtain it by determining all possible distances between a donor and acceptor ions in the crystal, and adding the value of c_{ET} (c_{EBT}) divided by r^6 for all distances. As can be expected, the energy back transfer has a positive contribution to the excited fraction of donor ions, whereas it has a negative contribution to the excited fraction of acceptor ions.

At low excitation power, we can consider the number of ions in the ground state as constant and the fraction of excited ions much smaller than 1: $x \ll 1$, which results in $(1-x) \approx 1$. Furthermore, we can set the total rates of donor and acceptor ions equal to an effective rate k, giving:

$$-k_{\mathrm{Yb_{eff}}}x_{\mathrm{don}} = -k_{\mathrm{don}}x_{\mathrm{don}} - W_{\mathrm{ET}}x_{\mathrm{don}}X_{\mathrm{acc}} + W_{\mathrm{BT}}x_{\mathrm{acc}}X_{\mathrm{acc}} \tag{2.24}$$

$$-k_{\mathrm{Er_{eff}}}x_{\mathrm{acc}} = -k_{\mathrm{acc}}x_{\mathrm{acc}} + W_{\mathrm{ET}}x_{\mathrm{don}}X_{\mathrm{don}} - W_{\mathrm{BT}}x_{\mathrm{acc}}X_{\mathrm{don}} \tag{2.25}$$

At high concentrations of both donor and acceptor ions, the migration and energy transfer processes are so fast that the excitation travels over many ions. Therefore it senses an average environment of acceptor and donor ions. This gives rise to the same effective rate for the donor and acceptor ions: $k_{\mathrm{Yb_{eff}}} = k_{\mathrm{Er_{eff}}}$.

$$-k_{\mathrm{eff}} = -k_{\mathrm{don}} - W_{\mathrm{ET}}X_{\mathrm{acc}} + W_{\mathrm{BT}}\frac{x_{\mathrm{acc}}}{x_{\mathrm{don}}}X_{\mathrm{acc}} = -k_{\mathrm{acc}} + W_{\mathrm{ET}}\frac{x_{\mathrm{don}}}{x_{\mathrm{acc}}}X_{\mathrm{don}} - W_{\mathrm{BT}}X_{\mathrm{don}} \tag{2.26}$$

$$-k_{\mathrm{eff}} = \frac{1}{2}\Big(k_{\mathrm{acc}} + k_{\mathrm{don}} + X_{\mathrm{don}}W_{\mathrm{BT}} + X_{\mathrm{acc}}W_{\mathrm{ET}} - \sqrt{(k_{\mathrm{acc}} + k_{\mathrm{don}} + X_{\mathrm{don}}W_{\mathrm{BT}} + X_{\mathrm{acc}}W_{\mathrm{ET}})^2 - 4(k_{\mathrm{don}}X_{\mathrm{don}}W_{\mathrm{BT}} + k_{\mathrm{acc}}(k_{\mathrm{don}} + X_{\mathrm{acc}}W_{\mathrm{ET}}))}\Big) \tag{2.27}$$

This effective rate depends on the balance between energy transfer and energy back transfer as well as the concentration of acceptor and donor ions and their individual radiative rates. So at high concentrations where migration is fast, the decay curve will behave as a single exponential function.

2.5 Monte Carlo Simulations

As discussed previously, Monte Carlo simulations can be used to model a crystal in which migration plays an important role. Monte Carlo simulations are based on repeated random sampling to obtain numerical results. The simulated crystals are built around the microscopic properties of the crystal system and by repeating the simulations a large number of times and averaging, a description of the macroscopic behavior of the excited state can be obtained. In this section, the details and important parameters of Monte Carlo simulations will be discussed.

2.5.1 Periodic boundary conditions

We want the simulated system to mimic the real system as good as possible. A simulated system however always has a finite size. As a consequence, there will be ions at the edge of the crystal that have fewer neighbor ions then the ones in the center of the crystal. In a real system, we deal with large crystals in which the surface area is low compared to the volume. This is why we implement periodic boundary conditions, which can be visualized as a repetition of the crystal in space. Translated to the simulation, this implies that the box size length will be subtracted from the distance between two ions if the distance is bigger than a half of the box size length. This is done for all three dimensions. In practice this means that an ion near the bottom left edge of our simulated crystal will also interact with ions near the top right edge.

2.5.2 Repetition of simulations and box size

Two important parameters regarding Monte Carlo simulations are the number of repeated simulations and the box size of every simulation. A huge amount of simulations or a very large box size will result in an unnecessarily long computation time. That is the main reason why we do not want our system to be too big. On the other hand, we cannot make it too small either. If we were to simulate only one crystal, there is a possibility that this system contains "special" configurations. These special configurations can be clusters of ions or isolated ions and can have a big influence on the final decay curve. That is why we simulate multiple crystals, so the average configuration is truly random. Furthermore, the outcome can be inadequate if the box size is smaller than the distance over which an excitation can migrate. If this is the case, we would cut off certain interactions in the simulation and this would be a wrong representation of the real system. To check how big the box size should be, one can simulate a crystal of different sizes and check when the outcome of the simulation converges. If a further increase in box size does not give a different result, one can be sure that the box size is big enough. By tuning the number of simulations and the box size, we can model a physically relevant system while limiting computing time and power.

3 Experimental Section

The Yb^{3+} and Er^{3+} doped Gd_2O_2 micro-crystalline samples used for all the luminescent measurements were made by Leuchtstoffwerk Breitungen GmbH (Breitungen, Germany), which have experience in the synthesis of high quality Gd_2O_2 doped with lanthanides. Excitation spectra and decay curves were measured on the spectrofluorometer (Edinburgh Instruments FLS 920) using an optical parametric oscillator (OPO) system (Opotek Opolette 355 type II) pumped by the third harmonic of a Nd:YAG laser as excitation source. This OPO system offers a continuous tunable optical range from 410 to 2200 nm, a maximum energy of 1.8 mJ per pulse in the infrared region, a pulse length of 7 ns, and a repetition rate of 20 Hz. The N_2-cooled Hamamatsu R5509-72 photomultiplier tube was used for detection in the infrared region. For the upconversion experiments, a 2 W continuous wave laser of 980 nm was used as an excitation source. The visible light was detected by a Hamamatsu R928 PMT with a grating blazed at 500 nm.

For the simulated decay curves, Monte Carlo simulations that rely on a random number generator were used. In the simulations, a crystal lattice is simulated that has available lattice sites for dopant ions at fixed positions. The doping with Yb^{3+} and Er^{3+} ions takes place randomly. Both types of luminescent ions have a probability to get excited. When in the excited state, they can decay radiatively, or they can transfer their energy to other ions. The radiative decay rate depends on the type of ion and the energy transfer rate depends on the two types of ions involved in the transfer process and the distance between them. For each generated crystal, a subset of ions is brought to the excited state. After this, the rates of all possible processes are added up. With the help of random numbers and the likelihood of each process, one of these processes is picked and carried out. The system is then updated to its new configuration and again, all the rates are summed and a new process takes place. This will repeat itself until all the ions are back in the ground state. The time step between each process is determined by $-\frac{e^{(1-randomnr)}}{totalrate}$. To record the essential output of the simulations: the emission of photons over time, two histograms are created. One histogram for the donors and one for the acceptors. Every time a radiative transition takes place, we check the type of ion (donor or acceptor), and add a count to the corresponding histogram in the appropriate time bin. This way, we keep track of the photons emitted by the luminescent ions and can later visualize decay curves by plotting the histograms. For each simulation, 2000 crystals were generated that have a box size of 15x15x15. In appendix A, it was checked that the outcome of the simulated decay curves is converged for these parameters. At high concentrations (10% Yb^{3+} and 10% Er^{3+}), a cut-off distance of 0.91 nm was introduced due to lack of computational power. This means that the interaction between ions that are separated a larger distance than 0.91 nm were neglected in the simulation.

4 Results and Discussion

4.1 Energy levels

To get a first impression of our system, it is convenient to map the energy levels of the Yb^{3+} and Er^{3+} luminescent ions. Since we are interested in the first steps of the upconversion process, the $^2F_{5/2}$ level of Yb^{3+} and the $^4I_{11/2}$ level of Er^{3+} are of interest. The energy of the photons needed to bridge the gap between these levels and the ground state is approximately 980 nm. The exact energy differences between states can be extracted from excitation spectra. These spectra will also come to use in determining the most efficient excitation wavelength.

Figure 5 shows (a) the excitation of the $^2F_{5/2}$ level of Yb^{3+} and (b) that of the $^4I_{11/2}$ level of Er^{3+}. For Yb^{3+}, a 15% doped sample was used and the emission was measured at 1030 nm. For Er^{3+}, a 10% doped sample was used and the emission of the lower lying $^4I_{13/2}$ level was measured at 1510 nm. Both spectra show a maximum in emission intensity around an excitation wavelength of 980 nm. The excitation lines in the spectrum of Er^{3+} are better defined. This is because Er^{3+} has multiple energy levels so we can measure the emission of a lower lying energy level than the one which we excite. Yb^{3+} on the other hand only has one energy level apart from the ground state. When measuring the excitation spectrum, we measure emission from the same level as the one we excite. Therefore, we have to detect at the lowest energy weak line and this weak signal results in less well defined excitation lines. Since lanthanide transitions typically exhibit no Stokes shift, we assume that the excitation and emission peaks lie at the same wavelengths. We therefore can conclude that there is a big spectral overlap between the emission of Yb^{3+} and the excitation of Er^{3+}. Since spectral overlap is one of the criteria for energy transfer, this is a positive outcome.

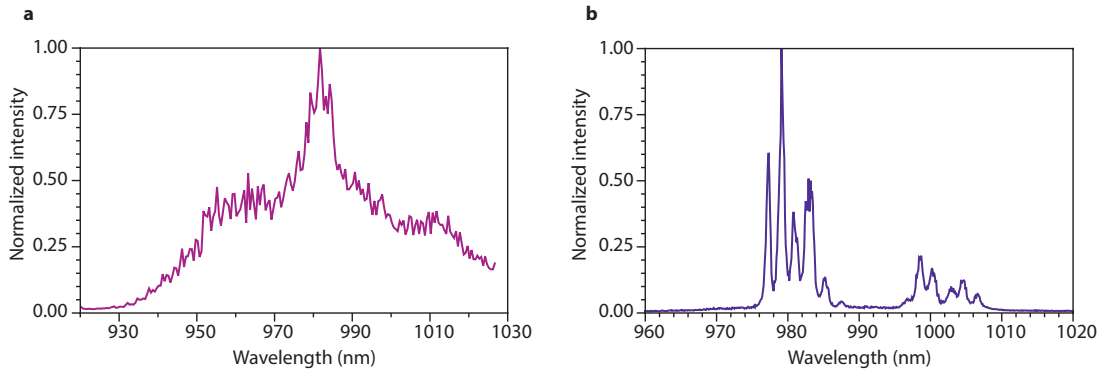

Figure 5: (**a**) Excitation spectrum of a $Gd_2O_2S:Yb^{3+}$(15%) sample, excited from 920-1027 nm. The emission was detected at 1030 nm. (**b**) Excitation spectrum of a $Gd_2O_2S:Er^{3+}$(10%) sample, excited from 930-1040 nm. The emission of the lower lying $^4I_{13/2}$ level was measured at 1510 nm.

4.2 Lifetimes Single Doped Crystal System

4.2.1 Reabsorption

As was discussed in the theoretical section, the decay times of the luminescent ions can give us information about the energy processes taking place in the samples. As a starting point, we will need to know the intrinsic decay times of our single doped samples: $Gd_2O_2S:Yb^{3+}$ and $Gd_2O_2S:Er^{3+}$. We however first need to check if reabsorption takes place. Figure 6 shows the influence of diluting on the lifetime of a luminescent sample. For a $Gd_2O_2S:Yb^{3+}$(10%) sample, the decay curves of samples with different weight-percentages were measured. All the decay curves were fit to a mono-exponential function. At first, diluting with $BaSO_4$ results

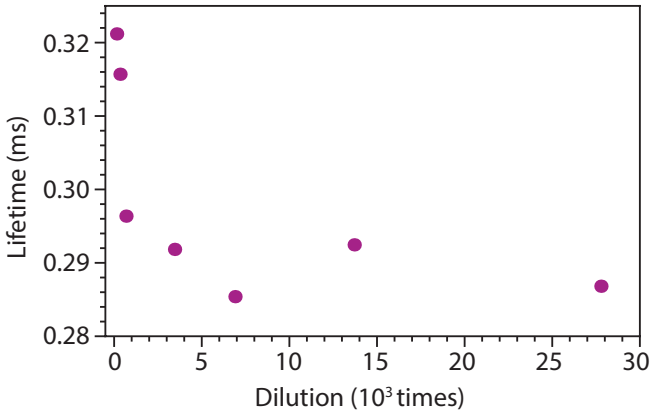

Figure 6: The influence of diluting with $BaSo_4$ on a Gd_2O_2S:Yb^{3+}(10%) sample.

in a shorter lifetime. As discussed in section 2.4.1, we can ascribe the longer lifetimes in less diluted samples to reabsorption. From 3500 times diluted onward, a further dilution does not cause a further decrease in lifetime. At this point, we can assume that reabsorption no longer takes place. In all the experiments that will follow in this thesis, we will make sure that reabsorption is negligible by diluting the samples with $BaSO_4$.

4.2.2 Lifetime and concentration quenching

Figure 7 shows the lifetime of single-doped samples of (a) different concentrations Yb^{3+} and (b) different concentrations Er^{3+}. For both types of ions, the lifetime decreases as the concentration increases. This can be ascribed to concentration quenching. At higher concentrations, the migration of an excitation can be fast since ions are close together. With this, the probability that the energy will reach a trap and is lost via non-radiative relaxation increases as well. These traps are often defects in the crystal system. For the 15%-doped samples, the decrease in lifetime is only 9% for the Yb and 16% for the Er samples compared to the 0.1%-samples. This demonstrates that almost no quenching takes place and is an indication for a very high quality of the crystal samples. Because of concentration quenching at high concentrations, we base the intrinsic rates of donor and acceptor ions on the lifetimes we find for low concentrated samples (0.1%). This results in a intrinsic rates of $\gamma_{\mathrm{Yb}} = \frac{1}{\tau_{\mathrm{Yb}}} = \frac{1}{0.29} = 3.45\ \mathrm{ms}^{-1}$ and $\gamma_{\mathrm{Er}} = \frac{1}{\tau_{\mathrm{Er}}} = \frac{1}{1.95} = 0.51\ \mathrm{ms}^{-1}$.

4.3 Energy Transfer

To determine the energy transfer (ET) strength, we investigate a double-doped crystal. It is best to look at a system with a low concentration of donor ions because at a low donor ion concentration, we can assume that the donors are too far away from each other for migration to play an important role. The decay of the donors can then be described as in equation 2.12. Figure 8 visualizes (a) the dependency on acceptor concentration and (b) the dependency on energy transfer strength of the donor decay. For both an increasing acceptor concentration and increasing energy transfer strength, the decay of the donor ions becomes faster. This is what we expect since the higher the probability of energy transfer is, the faster the population of excited donor shrinks, so the faster the decay will be.

Figure 9 shows the measured decay curve of a low doped sample: Gd_2O_2S:Yb^{3+}(0.1%)Er^{3+}(1%). To avoid upconversion, the excitation density was kept low by placing a neutral density filter of 0.025% between the laser and the sample. In the

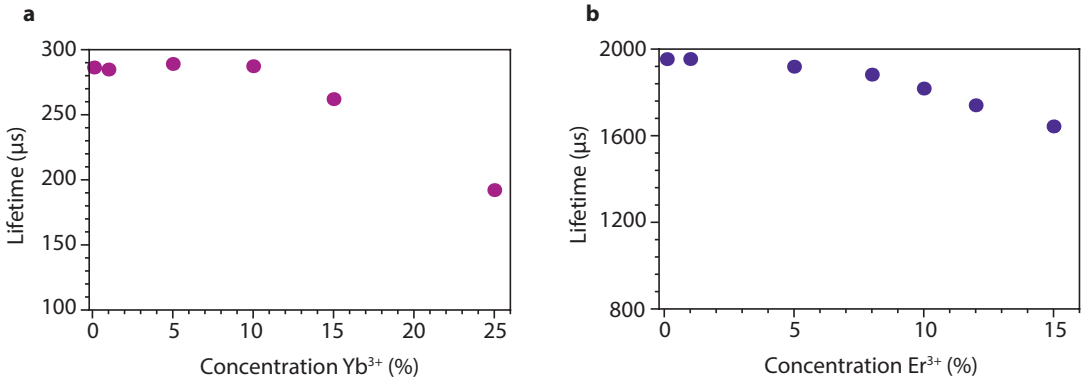

Figure 7: Measured lifetimes of different concentrations of (**a**) single doped $Gd_2O_2S:Yb^{3+}$ and (**b**) single doped $Gd_2O_2S:Er^{3+}$. All samples were diluted with $BaSO_4$ so reabsorption did not take place. As the concentration increases, the lifetime decreases as a consequence of concentration quenching.

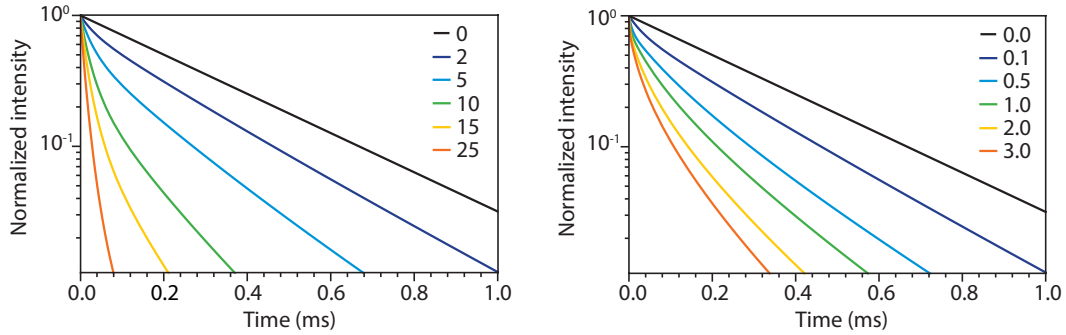

Figure 8: The theoretical decay curves of the donor emission for different acceptor concentrations and energy transfer strengths. The radiative rate was set to 3.45 ms^{-1}. (**a**) The energy transfer strength was set to 0.1 $ms^{-1}nm^6$ and the different acceptor concentrations are: 0% (black), 2% (purple), 5% (blue), 10% (green), 15% (yellow), 25% (orange). (**b**) The acceptor concentration was set to 2% and he different energy transfer strengths are: 0.0 (black), 0.1 (purple), 0.5 (blue), 1.0 (green), 2.0 (yellow), and 3.0 $ms^{-1}nm^6$ (orange).

first millisecond after the laserpulse, we observe the same peculiar shape as the in theoretical description of the donor emission. We also observe a longer component in the decay curve. We can ascribe this long component to Er^{3+} (acceptor) emission. In the experiments, it is not possible to measure purely donor or acceptor decay, because the two have a big spectral overlap. That is why we will measure emission from both the donors (Yb^{3+}) and the acceptors (Er^{3+}) in every decay curve. Because equation 2.12 only describes the behavior of the donor emission, we have to add at least one extra exponent to account for the emission of acceptor ions, before we can properly fit the experimental data:

$$I(t) = A_1 e^{-\gamma_{Yb} t} \prod_{i}^{\text{shells}} (1 - \phi + \phi e^{-ct/r_i^6})^{n_i} + A_2 e^{-\gamma_{Er}}. \tag{4.1}$$

Since we know the radiative lifetime of the donors, the acceptor concentration, and have the neighbor-list of our crystal host, we can fit our experimental data to equation 4.1 to obtain the energy transfer strength. The best fit to this equation is shown as a solid line in figure 9. From the fit, we extract an energy transfer parameter of 3.71 ms^{-1} nm^6. From the zoomed data in figure 9b, it is clear that the shape of the decay curve is in good agreement with the theoretical description of the decay.

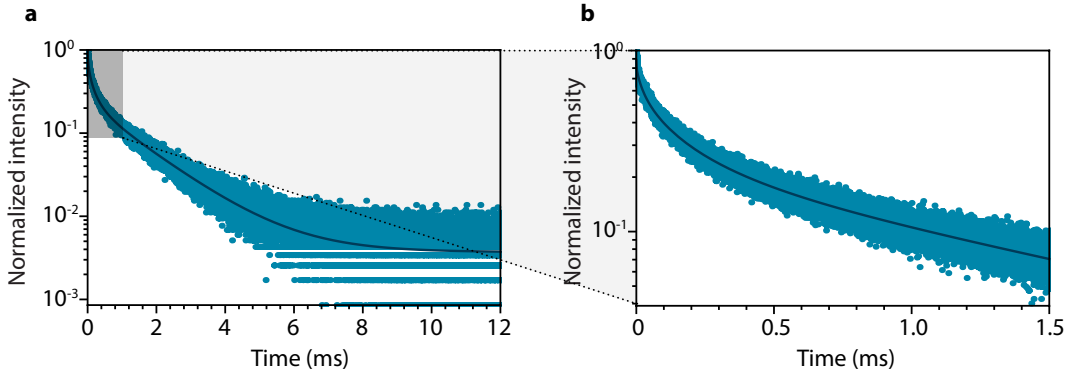

Figure 9: The measured decay curve of a Gd_2O_2S:Yb^{3+}(0.1%)Er^{3+}(1%) sample excited at 981 nm. The solid line shows the best fit of the data to equation 4.1. (**a**) The emission intensity up to 12 ms after the laser pulse. (**b**) The emission intensity up to 1.5 ms after the laser pulse, measured at a higher resolution.

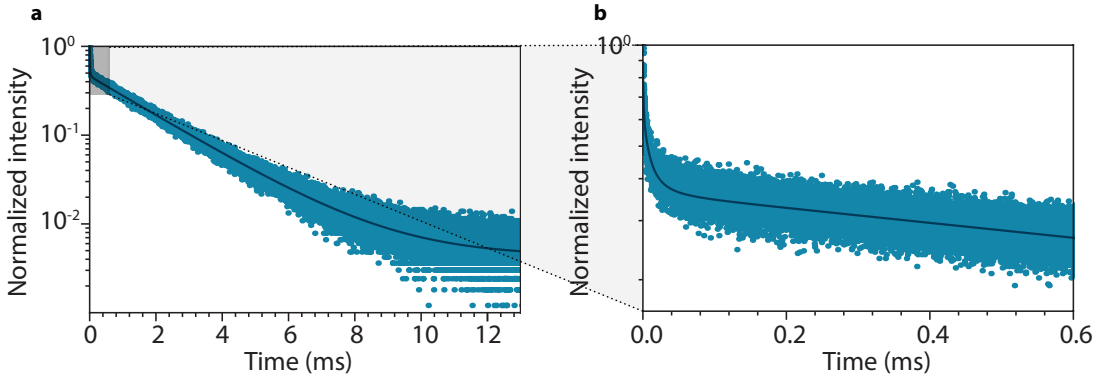

Figure 10: The measured decay curve of a Gd_2O_2S:Yb^{3+}(0.1%)Er^{3+}(5%) sample excited at 981 nm. The solid line shows the best fit of the data to equation 4.1. (**a**) The emission intensity up to 13 ms after the laser pulse. (**b**) The emission intensity up to 0.6 ms after the laser pulse, measured at a higher resolution.

Figure 10 shows the decay curve of a Gd_2O_2S:Yb^{3+}(0.1%)Er^{3+}(5%) sample. If we compare this data to figure 9, we observe a much faster decay right after the laser pulse. This is because of the higher acceptor concentration. When there are more acceptors present in a sample, there will be more energy transfer from donor to acceptor ions and this results in a faster decay of the donor ions. Using the value of 3.71 ms^{-1} nm^6 that we found for c_{ET} for a Gd_2O_2S:Yb^{3+}(0.1%)Er^{3+}(1%) sample, we can fit the experimental data to equation 4.1. The fit is shown as a solid line in figure 10. The fit gives a good description of the experimental data, so we can conclude that the value we found for the energy transfer strength is adequate.

Using equation 2.4 and the energy transfer strength, we can calculate that the Förster radius is $r_0 = 1.01$ nm. If we compare this to values for other systems, e.g. 0.49 nm for a Ce^{3+}/Nd^{3+} system [31], we can conclude that the energy transfer is really efficient in our system. To get a better feeling for the value of the energy transfer strength, we can express the nearest-neighbor efficiency: $\eta^{NN} = \frac{k_{ET}^{NN}}{k_{ET}^{NN}+k_{rad}}$. In our host material, the closest distance possible between a donor and acceptor is 0.38514 nm. For this distance, we find a value of $\eta^{NN} = 0.997$. This means that if there is an acceptor ion at the closest distance from a donor ion, the probability that energy transfer will occur is really high, namely 0.997.

4.4 Energy Back Transfer

4.4.1 Simulated decay curves including EBT

Thus far we have found values for the intrinsic rates of the donors and acceptors, and for the energy transfer strength. We will now study more relevant systems, with a high concentration of Yb^{3+} and Er^{3+}. At high concentrations, the system becomes more complex because migration and energy transfer from acceptors back to donors play an important role. In addition, the spectral overlap between the donor and acceptor emission spectra makes it impossible to measure emission from the donors or the acceptors separately. For these reasons, we choose to first turn to simulations before we measure experimental data. This way, we will get a better understanding of the effect that certain processes have on the luminescence and this can help us with the analysis later on.

Figure 11 shows the simulated decay curves of (a) the Yb^{3+} ions and (b) the Er^{3+} ions of a Gd_2O_2S:Yb^{3+}(0.1%)Er^{3+}(1%) sample. The EBT strength was set to half of the ET strength ($c_{EBT} = \frac{1}{2}c_{ET} = 1.85$ $ms^{-1}nm^6$). The decay of the donor (Yb^{3+}) ions can no longer be fit to equation 2.12, because the possibility of EBT alters the decay of the donors. The shape of the first 0.5 ms of the donor decay curve is still similar to the shape of the decay without the possibility of EBT. However, at longer times after the laserpulse, the intensity of donor-emission in a crystal in which EBT can occur is much higher than in one without the EBT process. The persisting of the emission from donor ions can be ascribed to the EBT. We can amend for this effect by adding an extra exponent to the emission intensity when we fit the expression for donor decay to the simulated or experimental data. When EBT can happen, the decay of the donors can by described by:

$$I(t) = A_1 e^{-t/\tau_{Yb_1}} \prod_i^{\text{shells}} (1 - \phi + \phi e^{-ct/r_i^6})^{n_i} + A_2 e^{-t/\tau_{Yb_2}}. \tag{4.2}$$

The simulated decay curve of the donor ions was fit to this equation, as can be seen in figure 11a. We set the ET strength to 3.7 $ms^{-1}nm^6$ and τ_{Yb_1} to 0.29 ms; the intrinsic lifetime of the donors. This gave a value of $\tau_{Yb_2} = 1.02$ ms. This lifetime is much longer than the lifetime of a single doped Yb^{3+}-sample and accounts for the emission milliseconds after the laser pulse.

The simulated decay curve of the acceptor (Er^{3+}) ions shows an initial rise, followed by exponential decay, as is depicted in figure 11b. The rise time is because the initial excitation is on the donor ions. Energy has to be transferred to the acceptor ions before they can emit. The

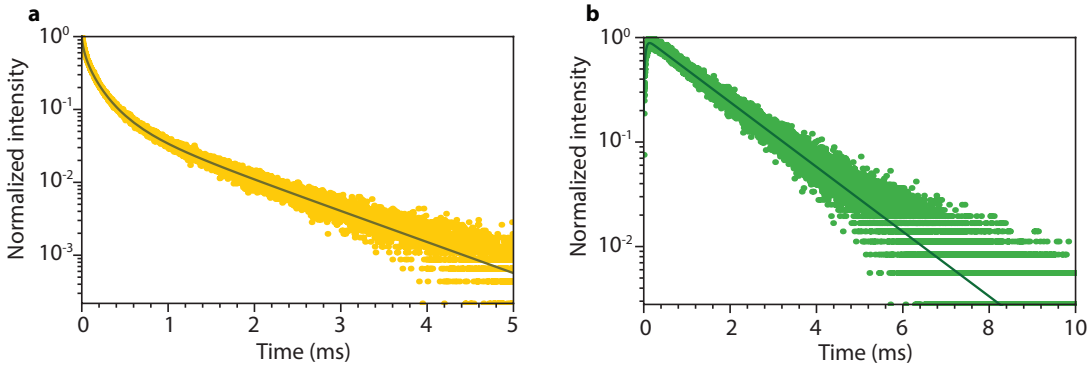

Figure 11: The simulated decay curves and their fits of a Gd_2O_2S:Yb^{3+}(0.1%)Er^{3+}(1%) sample, in which EBT can take place. The radiative rates were set to $\gamma_{Yb} = 3.45 ms^{-1}$ and $\gamma_{Er} = 0.51 ms^{-1}$. The EBT strength was set to half of the ET strength $c_{EBT} = \frac{1}{2}c_{ET} = 1.85$ $ms^{-1}nm^6$. (**a**) The simulated decay curve of Yb^{3+} and its fit to equation 4.2 (solid line). (**b**) The simulated decay curve of Er^{3+} and its fit to a biexponent (solid line).

simulated decay of the acceptors was fit to a bi-exponent. This gave a risetime of $\tau_{rise} = 0.04$ ms and a lifetime of $\tau_{Er} = 1.40$, which is shorter than the lifetime of a single doped Er^{3+}-sample. The EBT process thus shortens the lifetime of the acceptor ions.

4.4.2 Simulated effect of EBT on the lifetime of acceptor ions

Intuitively, one can understand that the strength of energy back transfer will have an influence on the lifetime of the acceptor ions. If energy back transfer is likely to occur, the acceptors are more likely to lose their energy by transferring it back to the donors and therefore, the lifetime of acceptor ions becomes shorter. To support this hypothesis, we simulated decay curves for different values of the EBT.

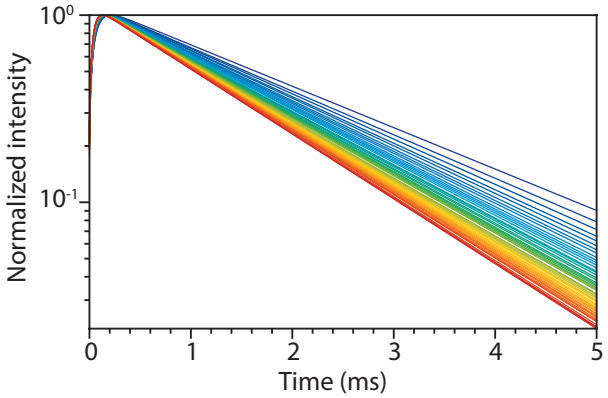

Figure 12: The resulting biexponential fits to the simulated decay curves of the acceptor ions in a Gd_2O_2S:Yb^{3+}(0.1%)Er^{3+}(1%) sample. The ET strength was set to 3.7 $ms^{-1}nm^6$ and the EBT strength was varied from 0 (blue) to 3.7 (red) in steps of 0.074 $ms^{-1}nm^6$.

Figure 12 shows the resulting fits to the simulated acceptor (Er^{3+}) decay curves of a Gd_2O_2S:Yb^{3+}(0.1%)Er^{3+}(1%) sample for different values of the EBT. We used a bi-exponent to fit the simulated data of Er^{3+} emission. Again, since the initial excitation is on the donor (Yb^{3+}) ions, energy transfer has to occur before the acceptor ions become excited. As a result,

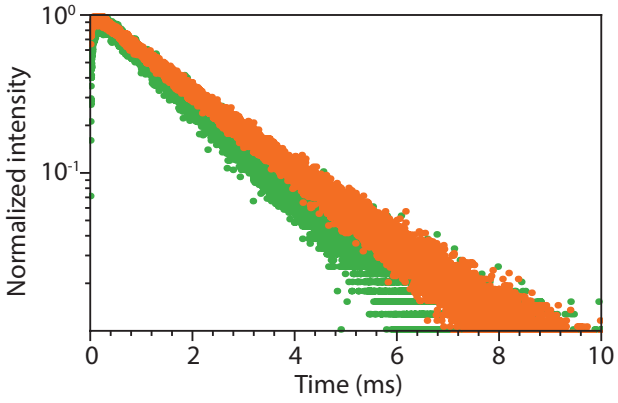

Figure 13: Simulated decay curves of the acceptor ions in a crystal doped with 0.1% Yb^{3+} and 1% Er^{3+} for different excitation possibilities. The excitation was set to donor ions only (green) and both donor and acceptor ions (orange). The possibility of acceptor excitation resulted in a longer lifetime of the acceptor ions.

the emission intensity shows a rise at the beginning. The second component of the decay curve can be attributed to the actual lifetime of the excited state and depends on the energy back transfer strength, as can clearly be seen from the figure. A higher energy back transfer strength results in a shorter lifetime of the Er^{3+} ions. This can be explained by the fact that a larger energy back transfer strength gives a higher rate for energy back transfer. Since the radiative rate is unaltered, this will result in a shorter lifetime.

4.4.3 Effect excited fraction of acceptor ions on their lifetime in simulations

Because of the dependence of the EBT-strength on the lifetime of Er^{3+}, one could imagine that measuring the lifetime of Er^{3+} can be a proper experiment to obtain a value for the EBT-strength. However, before we can link the acceptor lifetime to the EBT strength, we have to exclude the influence of the excited fraction of Er^{3+} ions. In the simulations, we can easily set the excitation to only Yb^{3+} ions. In practice however, we will always excite the Er^{3+} ions as well. Since we are measuring in the low concentration regime so no migration takes place, the fraction of excited Er^{3+} could have an effect on the lifetimes. To investigate if the excited fraction of Er^{3+} ions indeed has an influence on the acceptor lifetime, we simulated the decay curve for acceptor ions for a crystal in which only donor ions are excited, and for a crystal in which both donor and acceptor ions are excited. Figure 13 shows the outcome of these simulations. The green curve shows the acceptor decay when only donor ions are excited and the orange curve shows the acceptor decay when both donor and acceptor ions are excited. When we compare the two decay curves of acceptor ions, we see that the lifetime is indeed different. The lifetime of acceptor ions is longer when they have a chance to get excited.

4.4.4 Effect excited fraction of acceptor ions on their lifetime in experiments

We will now focus on the experimental data again to test if the excited fraction of acceptor ions also plays an important role in practice. In order to test this, we fix the emission wavelength at which we measure the decay curve of a Gd_2O_2S:Yb^{3+}(0.1%)Er^{3+}(1%) sample at 1020 nm and scan over multiple excitation wavelengths. An example of one of the measured decay curves is shown in figure 14. Based on the lifetimes we found earlier for donor and acceptor ions, we assume that the lifetime of the acceptor (Er^{3+}) ions is the longest. To extract the lifetime of the

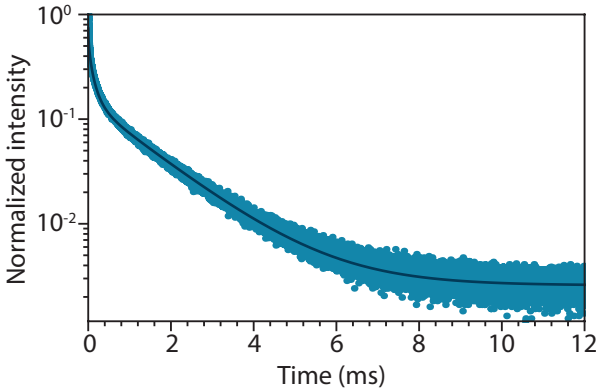

Figure 14: Measured decay curve of a Gd_2O_2S:Yb^{3+}(0.1%)Er^{3+}(1%) sample excited at 998.8 nm. The emission wavelength was set to 1020 nm at which both Yb^{3+} and Er^{3+} emission are detected. The data was fit to equation 4.3 (solid line).

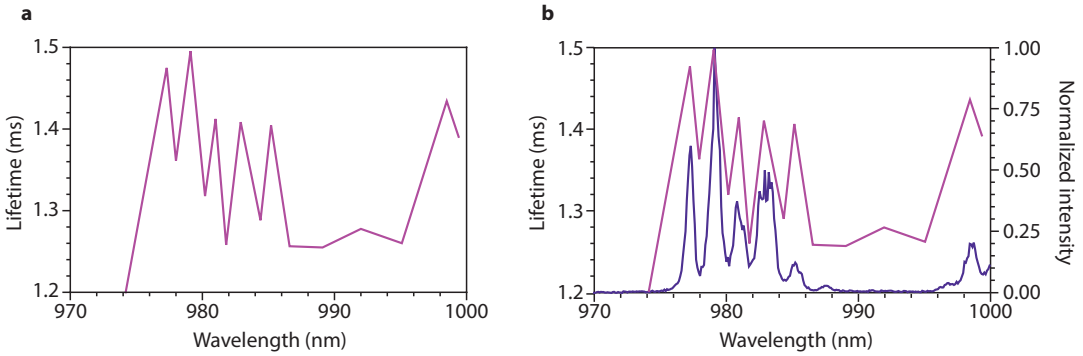

Figure 15: (**a**) The lifetime of the long component in the decay curve of a Gd_2O_2S:Yb^{3+}(0.1%)Er^{3+}(1%) sample as a function of the excitation wavelength. The variation in the lifetime is about 20%. (**b**) The lifetime of the long component plotted in the same graph as the excitation spectrum of the acceptor ions. The lifetime are the longest for wavelengths at which the direct excitation of acceptor ions is strongest.

acceptor ions from the measured decay curve, we fit the data to

$$I(t) = A_1 e^{-t/\tau_{\mathrm{Yb}}} \prod_i^{\text{shells}} (1 - \phi + \phi e^{-ct/r_i^6})^{n_i} + A_2 e^{-t/\tau_{\mathrm{Er}}}. \tag{4.3}$$

It may seem ambiguous that this equation resembles equation 4.2. We however have to keep in mind that contrary to the simulations, we cannot separate Yb^{3+} and Er^{3+} emission in the experiments. We choose to exclude the longer component of the lifetime of Yb^{3+} ions from the fit since its intensity is much lower than the intensity of Er^{3+} emission. The fit is displayed in figure 14 and gave a value of $\tau_{\mathrm{Er}} = 1.43$ ms. Because of EBT, this lifetime is shorter than the intrinsic lifetime of the acceptor ions.

Decay curves measured at different excitation wavelengths were fit like the one in figure 14. The resulting lifetimes of the long component are plotted in figure 15. The variation in the lifetime is about 20%. If we want to relate the lifetime to the amount of excited Er^{3+} ions, it is interesting to compare the lifetimes at different excitation wavelengths with the excitation spectrum of Er^{3+}. These two data are plotted together in figure 15b. As can clearly be seen, the lifetimes are the longest for the wavelengths at which the direct excitation of Er^{3+} is strongest.

The difference in lifetime can be explained as follows. When the excitation is set to Yb^{3+} ions only, energy transfer has to occur before Er^{3+} emission can be seen. This means that the

emission from Er^{3+} ions that we see, will only come from the Er^{3+} ions that are near Yb^{3+} ions. These ions will have a higher probability to give their energy back to Yb^{3+} because of the small separation between them and the Yb^{3+} ions. Therefore, exciting in this fashion will predominantly give emission from Er^{3+} ions with a shorter lifetime. When the Er^{3+} ions get excited as well, the acceptor emission we measure can also come from acceptor ions further away from donor ions. These ions have a slower energy transfer rate due to their larger distance from donor ions and therefore have a longer lifetime.

4.4.5 The effective rate

If we want to get around the influence of the excited fraction of Er^{3+} on the lifetime, we can go to concentrations of 5% donor and acceptor ions or higher. In this regime, we can assume that energy migration and transfer processes occur relatively fast compared to radiative decay so any biased initial excitation density should average out. To check if this is indeed true, we can measure the lifetime of a Gd_2O_2S:Yb^{3+}(10%)Er^{3+}(10%) co-doped sample using different excitation wavelengths. In figure 16, an example of one of the measured decay curves is shown. The decay is mono-exponential and the fit gave a value of $\tau = 0.40$ ms.

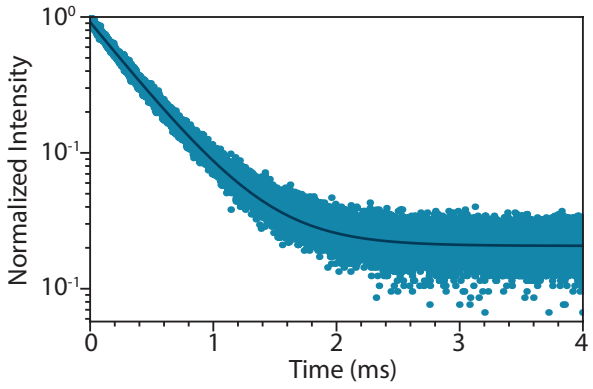

Figure 16: A measured decay curve of a Gd_2O_2S:Yb^{3+}(10%)Er^{3+}(10%) sample excited at 974 nm. The data was fit to a single-exponential function (solid line).

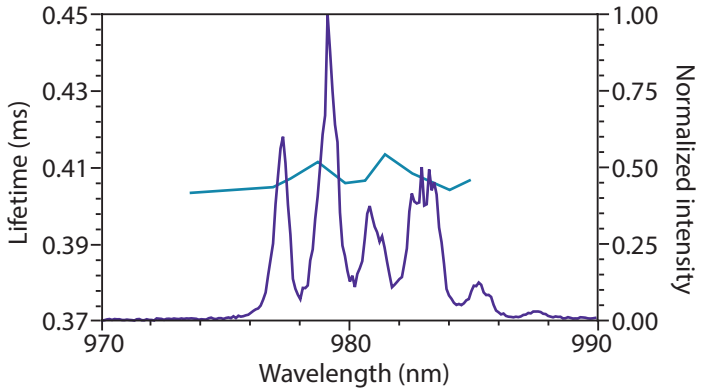

Figure 17: The lifetimes of a Gd_2O_2S:Yb^{3+}(10%)Er^{3+}(10%) sample at different excitation wavelengths plotted together with the excitation spectrum of the acceptor ions. The deviation in the lifetime is only 2.5% and there is no correlation with the excitation spectrum.

For different excitation wavelengths, the lifetime of the sample was fit and the results are shown in figure 17 together with the excitation spectrum of Er^{3+}. The deviation in the lifetime is much smaller than we saw before for a Gd_2O_2S:Yb^{3+}(0.1%)Er^{3+}(1%) sample. Furthermore, there is no relationship between the excitation spectrum of Er^{3+} and the measured lifetime anymore. This confirms that at high concentrations, the initial distribution of excited ions has no influence on the measured decay time.

The question now is how we can link the measured decay time at high concentrations to the energy back transfer strength. To answer this question, we can make use of equation 2.27, which describes the theoretical effective rate as a function of ET and EBT strength, donor and acceptor concentration and their individual radiative rates. In figure 18, the value of the theoretical effective rate is plotted against the concentration of acceptor ions for different values of the EBT strength. We see that for a system without acceptor ions (intersection with the y-axis), the effective rate is equal to the intrinsic decay rate of Yb^{3+} ions. This is of course what can be expected. For high acceptor concentrations, the effective rate becomes slower and is more similar to the rate of Er^{3+} ions. Furthermore, the effective rate becomes faster as the EBT strength is increased.

To get a value for the EBT strength, we measure the effective rate of samples with different concentrations Yb^{3+} and Er^{3+}. In figure 19, the measured rates of different samples are plotted against the acceptor concentration. The trend in the experimental data is different from the theoretical description in figure 18. The difference can be explained by two reasons. The first one is that at a low concentration, our assumption of fast migration may not be true. If this assumption does not hold, we cannot use the expression for the effective rate, and therefore the data points of low concentrations are of no use to us. If we for example look at the decay curve of the Gd_2O_2S:Yb^{3+}(1%)Er^{3+}(1%) sample, we do not observe a monoexponetial decay. This is a sign that the migration is limited and therefore no average environment is sensed by the excitation. The second reason of the deviation of the data from the theoretical description is due to concentration quenching at high concentrations. When measuring the lifetime of

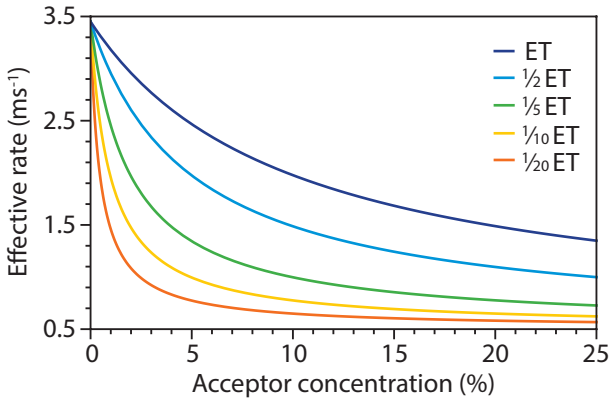

Figure 18: The effective rate according to equation 2.27 plotted against the acceptor concentration for different values of the EBT strength. The concentration of Yb^{3+} ions was set to 10% and the different values for EBT are: $\frac{1}{20}$ET (orange), $\frac{1}{10}$ET (yellow), $\frac{1}{5}$ET (green), $\frac{1}{2}$ET (blue), ET (purple).

single doped crystals, we already saw the effect of concentration quenching around 15%. At high concentrations, migration is fast and in a double-doped crystal, an excitation can move over both types of ions. As a result, concentration quenching will play an important role and this results in a faster rate. The measured rates of samples with a high concentration may therefore be faster then they would be in a perfect crystal system.

Taking this into account, we chose to use all samples with 5% Er and 5% Yb to determine the EBT strength. The data points and corresponding fits are presented in figure 20. The

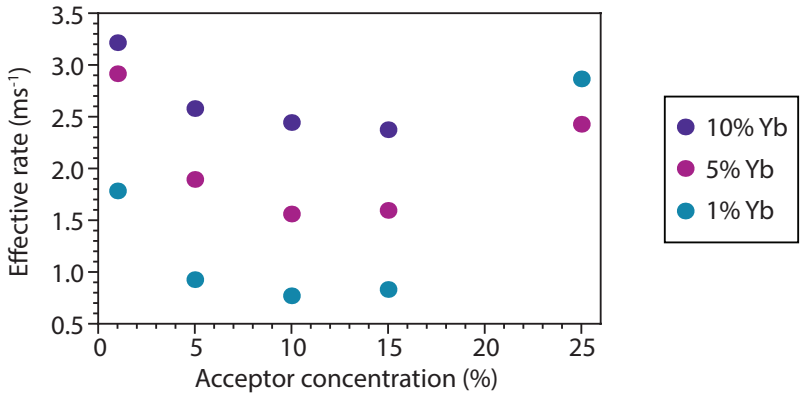

Figure 19: The measured effective rates for different concentrations of $Gd_2O_2S:Yb^{3+}Er^{3+}$ samples. An increase in acceptor concentration first results in a drop of the effective rate. Later, a further increase of acceptor concentration results in a acceleration of the effective rate.

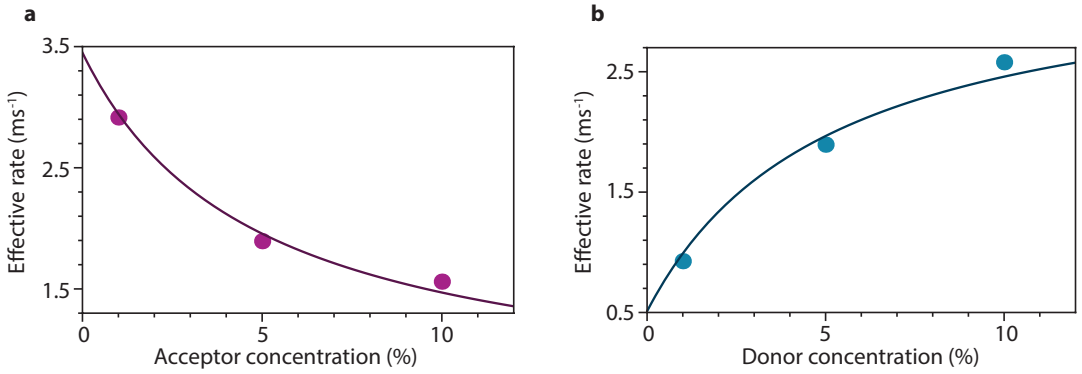

Figure 20: (**a**) The measured effective rates of a $Gd_2O_2S:Yb^{3+}(5\%)Er^{3+}(x\%)$ sample with x=1, 5 and 10%. (**b**) The measured effective rates of a $Gd_2O_2S:Yb^{3+}(x\%)Er^{3+}(5\%)$ sample with x=1, 5 and 10%. Both datasets were fit to the expression of the effective rate versus acceptor/donor concentration. The obtained EBT strengths are 3.61 for the 5% Yb^{3+} samples and 3.66 $ms^{-1}nm^6$ for the 5% Er^{3+} samples.

values for the EBT strength that we find are: 3.61 $ms^{-1}nm^6$ from the samples with 5% Er^{3+} and 3.66 $ms^{-1}nm^6$ from the samples with 5% Yb^{3+}. To conclude, we can state that the EBT strength almost has the same value as the one we found for the ET strength ($c_{ET} = 3.7$ $ms^{-1}nm^6$).

4.5 Migration

We have accurately determined the intrinsic rates of donor and acceptor ions, the energy transfer strength and the energy back transfer strength. The only parameters needed to make the modeling in the IR-region complete are the migration strengths. We will make use of simulations to examine the influence of migration over the two individual sublattices on the decay of the donors. Figure 21 shows simulated donor decay curves of a $Gd_2O_2S:Yb^{3+}(10\%)Er^{3+}(10\%)$ sample for different values of the donor-to-donor (c_{DD}) and acceptor-to-acceptor (c_{AA}) migration strengths. The striking resemblance between the three decay curves is that apart from the first 0.05 ms, they all have exactly the same lifetime. The difference in the first tens of microseconds is probably because of the cut-off distance in the simulation. Due to lack of computational power, we had to set the cut-off distance to 0.91 nm. This means that the interaction between ions that are separated a larger distance than 0.91 nm were neglected in the

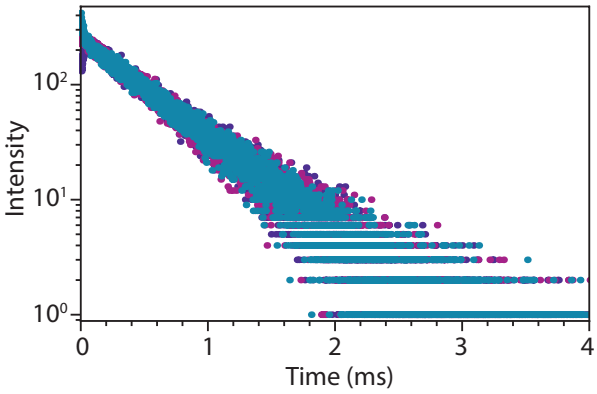

Figure 21: Simulated donor decay curves of a Gd_2O_2S:Yb^{3+}(10%)Er^{3+}(10%) sample for different values of the donor-to-donor and acceptor-to-acceptor energy migration. The energy migration strengths ($c_{DD} = c_{AA}$) were set to: 0 (purple), 3.7 (pink), and 37 ms^{-1} nm^6 (blue).

simulation. By introducing this cut-off distance, we strongly limit the energy transfer and energy migration in the crystal. The resulting decay curves however still provide us with useful information.

The presence of an effective rate namely tells us that migration must be fast. In section 4.4.5, we saw that fast migration is needed in order to obtain an effective rate of the system. When we neglect the first 0.05 ms of the simulated decay curves and fit them to a single exponential function, we get effective lifetimes of: 0.512 ms ($c_{DD} = c_{AA} = 0$), 0.504 ms ($c_{DD} = c_{AA} = 3.7$ $ms^{-1}nm^6$), and 0.513 ms ($c_{DD} = c_{AA} = 37$ $ms^{-1}nm^6$). We can compare these values to the theoretical effective rate that we would expect for this system. The theoretical effective rate of a Gd_2O_2S:Yb^{3+}(10%)Er^{3+}(10%) sample can be calculated using equation 2.27. When we use the same parameters as in the simulation, we obtain $k_{eff} = 1.961$ ms^{-1}. This results in a theoretical effective lifetime of $\tau_{eff} = 0.510$ ms, which corresponds really well with the simulated effective lifetimes.

The simulated decay curves show that even when the migration between the same type of ions is completely turned off, migration is nevertheless fast. From this we can conclude that the possibility of energy transfer and energy back transfer already leads to fast migration. Since the energy migration over the two individual sublattices has no influence on the resulting decay curves, we unfortunately cannot ascribe a specific value to the energy migration strengths.

4.6 Upconversion

Until now we have focused on the energy transfer processes that take place in the IR-region. It is nevertheless also interesting to look at the visible emission, since the ability of upconversion is what makes this system so valuable. The modeling of the extra energy transfer processes that get involved in the upconversion process is however complex so in this work, we will not try to assign values to these energy transfer strengths. Figure 22 shows emission spectra of different samples while exciting at 980 nm with a CW laser. Both the emissions from the $^2H_{11/2}$ and $^4S_{3/2}$ level around 550 nm (green) and the emission from the $^4F_{9/2}$ level at 670 nm (red) are measured. One has to be careful when comparing absolute intensities of different measurements, but since all the samples were prepared and measured in the same way, the absolute intensities can give us an impression of the most efficient upconversion concentrations and the trends present in the data.

As the concentration of Yb^{3+} ions is increased from 0.1% to 10%, the green and red emissions get more intense. A further increase of Yb^{3+} concentration to 15% and 25% results in a drop of emission intensity. The same holds for the concentration of Er^{3+}. At first, an increase

in concentration results in a higher intensity, and later, a further increase results in a drop of emission intensity. The optimum concentration of green Er^{3+} lies at 1% or 5%, depending on the concentration of Yb^{3+}. The drop in intensity at higher concentrations can be ascribed to concentration quenching. In section 4.5, we observed that the excitation can migrate over both type of ions because the rate of energy transfer and energy back transfer are fast compared to the radiative rates. This fast migration over both type of ions contributes to concentration quenching. The highest intensity is observed for the sample doped with 10% Yb^{3+} and 5% Er^{3+}.

When we examine the emission spectra of different concentrations of Er^{3+} in more detail, we notice that the ratio of the green and red peaks changes with the concentration. At high concentrations of Er^{3+} (15% and 25%), the green/red emission ratio becomes smaller. We observe this trend for different concentrations of Yb^{3+}. This change in ratio can be explained by the depopulation of the green emitting energy levels of Er due to cross-relaxation [33]. The relaxation energy from the $^2H_{11/2}$/ $^4S_{3/2}$ levels to the $^4I_{9/2}$ level corresponds with the excitation energy of the $^4I_{15/2}$ level to the $^4I_{13/2}$ level. Because of this, an Er^{3+} ion in the $^2H_{11/2}$ or $^4S_{3/2}$ level can transfer its energy to another Er^{3+} ion which is in its ground state. This process is called cross-relaxation. For cross-relaxation to happen, Er^{3+} ions need to be in close proximity. Therefore, cross-relaxation will have a higher probability to take place at higher concentrations and this leads to depopulation of the green emitting energy levels.

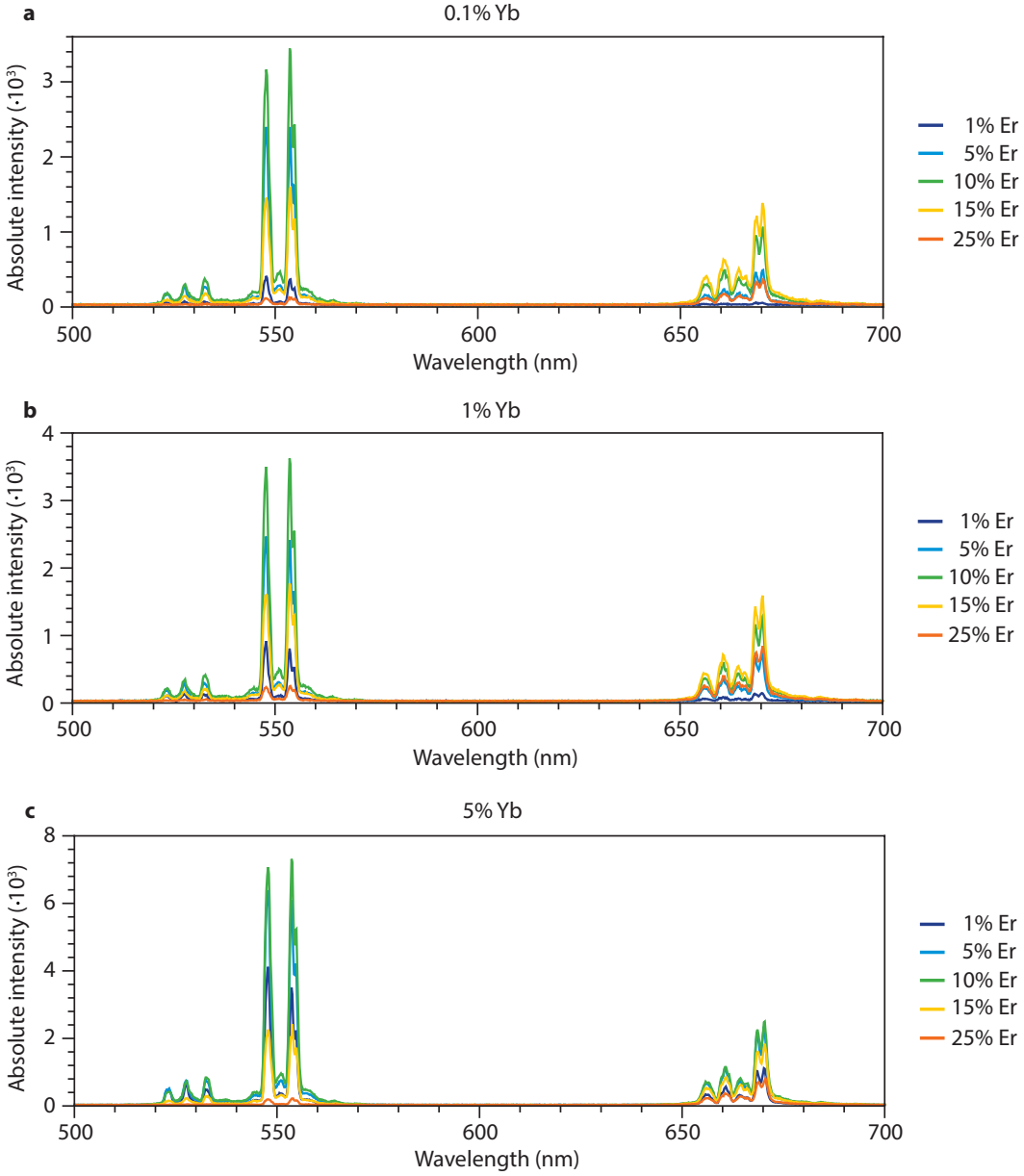
a
0.1% Yb
Absolute intensity (·10³)
Wavelength (nm)
1% Er
5% Er
10% Er
15% Er
25% Er
b
1% Yb
Absolute intensity (·10³)
Wavelength (nm)
1% Er
5% Er
10% Er
15% Er
25% Er
c
5% Yb
Absolute intensity (·10³)
Wavelength (nm)
1% Er
5% Er
10% Er
15% Er
25% Er

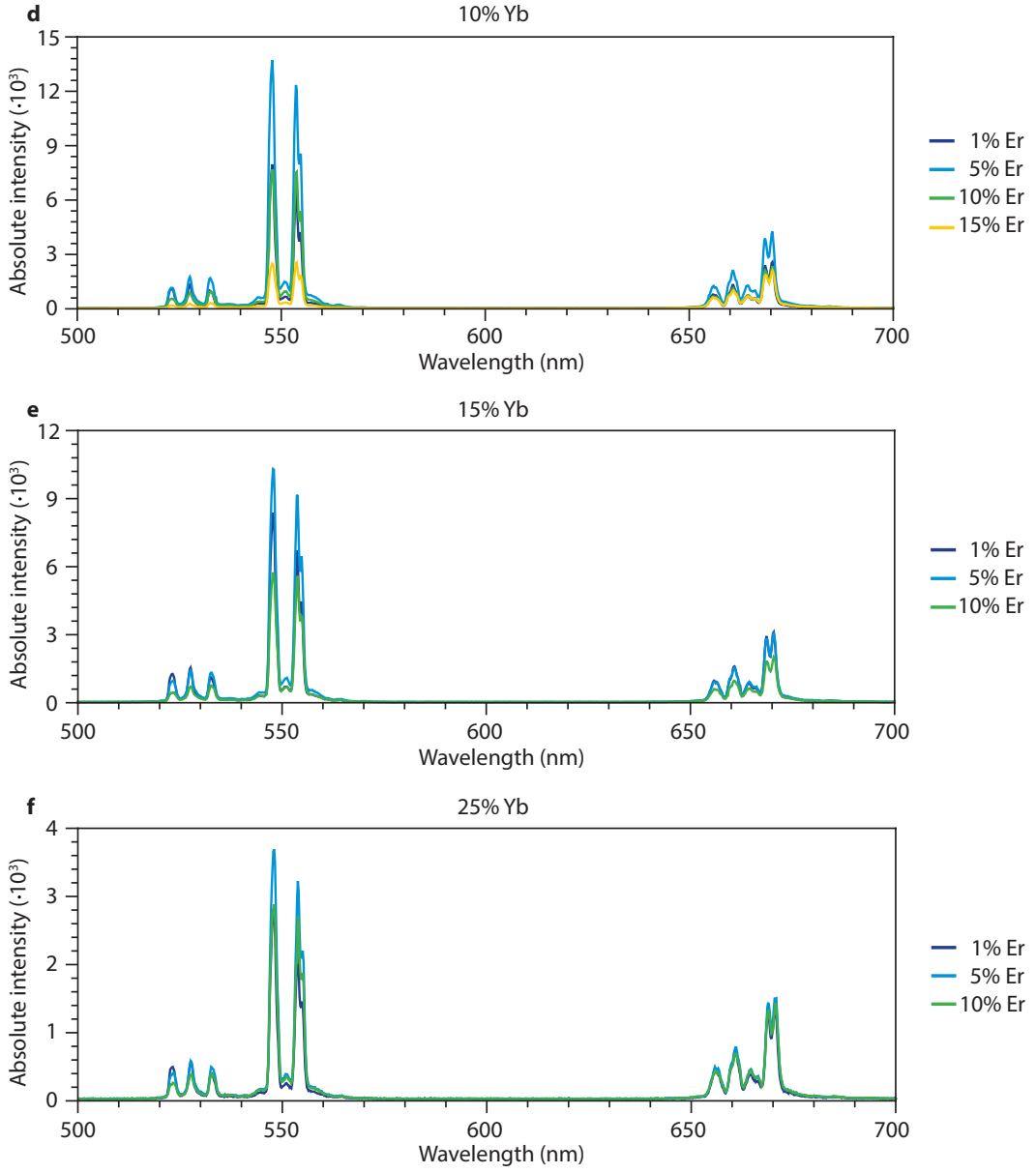

Figure 22: Upconversion emission intensities of the green and red emitting level for $Gd_2O_2O:Yb^{3+}Er^{3+}$ samples with different concentrations of donor and acceptor ions. A CW laser of 980 nm was used as excitation source.

5 Conclusion and Outlook

In this research, the processes accounting for the first steps towards upconversion in a $Gd_2O_2S:Yb^{3+}Er^{3+}$ system were investigated. Luminescence measurements on high quality micro-crystalline samples made by Leuchtstoffwerk Breitungen GmbH were performed. From these measurements, parameters were obtained for different processes taking place in the crystal. These parameters were used in Monte Carlo simulations to model the behavior of the luminescent ions in the crystal.

Luminescence decay curves of single doped samples were used to determine the intrinsic rates of the donor and acceptor ions. For 0.1 % samples, these values were measured to be γ_{Yb} = 3.45 ms^{-1} and γ_{Er} = 0.51 ms^{-1}. At high concentrations (>8% for Er^{3+} and >15% for Yb^{3+}), we observed concentration quenching.

Measurements on double doped crystals were performed to determine the energy transfer strength. A low concentration of donor ions was taken to exclude energy migration over the donors. The energy transfer strength we obtained from a $Gd_2O_2S:Yb^{3+}(0.1\%)Er^{3+}(1\%)$ sample was 3.7 $ms^{-1}nm^6$. This value for the energy transfer strength was able to properly fit the decay curve of a $Gd_2O_2S:Yb^{3+}(0.1\%)Er^{3+}(5\%)$ sample as well. The corresponding Förster radius of this energy transfer is $R_0 = 1.01$ nm.

To determine the energy back transfer strength, we measured multiple decay curves of samples with different concentrations. Samples doped with 5% Yb^{3+} ions and different Er^{3+} concentrations, and 5% Er^{3+} with different concentrations of Yb^{3+} were used. In this regime, energy migration and transfer processes are relatively fast compared to radiative decay. This results in an effective rate for the crystal. Fitting the values of the measured effective rate resulted in an EBT strength of 3.61 $ms^{-1}nm^6$ for the samples with 5% Er^{3+} and 3.66 $ms^{-1}nm^6$ for the samples with 5% Yb^{3+}. The EBT strength thus almost has the same value as the value we found for the ET strength, $c_{ET} = 3.7$ $ms^{-1}nm^6$.

Using the values we found for the intrinsic rates, the ET and EBT, we performed Monte Carlo simulations for different values of the donor-to-donor and acceptor-to-acceptor migration. The resulting decay curves all showed the same effective rate. This implies that migration is already fast due to energy transfer and energy back transfer. Since the energy migration showed no effect on the simulated decay curves, we were unfortunately not able to find a value for the donor-donor and acceptor-acceptor energy migration.

Upconversion experiments were performed to get an impression of the upconverting ability of the different concentrations. For both type of ions, we saw an optimum in the concentration. At concentrations higher than this optimum, the drop in emission intensity is caused by concentration quenching. Futhermore, the ratio of the green/red emission drops at higher concentrations of Er^{3+}. This is because cross-relaxation occurs at high Er^{3+} concentration (>15%) and this results in a depopulation of the green emitting states. The highest intensity of green emission was observed for the sample doped with 10% Yb^{3+} and 5% Er^{3+}.

The challenge that remains is to extend the model so it will be able to model the total upconversion process in a Yb^{3+}/Er^{3+} couple. The Monte Carlo simulation is written in such a way that upconversion can be implemented. The most difficult task however is to determine the parameters of the extra energy transfer processes. To examine these processes, a higher excitation density will be needed. Energy transfer from Yb^{3+} to an Er^{3+} in its excited place then can take place. However, energy transfer from Er^{3+} to another Er^{3+} ion can also lead to upconversion. Futhermore, we saw that cross-relaxation between Er^{3+} ions can also take place. These processes are only a few of all the possible processes that will have an influence on the upconversion. Therefore, it is important to try and separate these processes and first look at a single doped crystal containing only Er^{3+}. The Monte Carlo simulations can be used to predict the system's behavior and step by step, the parameters for the different processes can be determined.

6 Acknowledgments

The work presented in this thesis would not have been possible without the help of several people. Firstly, I would like to thank my daily supervisor, Freddy Rabouw. You put a lot of time in helping me with the spectroscopic measurements, the modeling of the system, analyzing the data, and coming up with new experiments. I really admire your creative and critical thinking and I learned a lot from you. You always gave me time to think about problems on my own but came to check upon me exactly when I needed you to. Furthermore, I would like to thank you for keeping me motivated. After every discussion we had, I got enthusiastic again. Secondly, I would like to thank Andries Meijerink for giving me the opportunity to perform my master thesis in the CMI group and for the supervision during this project. Our discussions about the results were very helpful to me. Special thanks Mathijs, Pedro and Tim. You were always willing to answer one of my many questions and help me out with the experimental setup. Thanks to Paolo for helping me with the modeling. Sometimes, the debugging drove me insane but luckily you were around to help and calm me down. Thanks to Tim Prins for letting me join in on your promising research. It did not always go without a fight but I enjoyed working with you so much and I am looking forward to write it all down. Finally, I would like to thank all students and staff members of the CMI group. I had a really pleasant time the past 1.5 year and you all contributed to that.

References

[1] T. Jüstel, H. Nikol, and C. Ronda. New developments in the field of luminescent materials for lighting and displays. *Angewandte Chemie*, 37:3084–3103, 1998.

[2] D.K. Chatterjee, A. J. Rufaihai, and Y. Zhang. Upconversion fluorescence imaging of cells and small animals using lanthanide doped nanocrystals. *Biomaterials*, 29:937–943, 2008.

[3] C.G. dos Remedios and P.D.J. Moens. Fluorescence resonance energy transfer spectroscopy is a reliable "Ruler" for measuring structural changes in proteins: Dispelling the problem of the unknown orientation factor. *Journal of Structural Biology*, 115:1, 1995.

[4] G. S. Yi and G. M. Chow. Sunthesis of hexagonal-phase $NaYF_4$:Yb,Er and $NaYF_4$:Yb,Tm nanocrystals with efficient up-conversion fluorescence. *Advanced Functional Materials*, 16:2324–2329, 2006.

[5] Y. Wang, X. Guo, S. Liu, K. Zheng, G. Qin, and W. Qin. Controllable synthesis of beta-$NaLuF_4$:Yb^{3+}, Er^{3+} nanocrystals and their application in polymer-based optical waveguide amplifiers. *Journal of Fluorine Chemistry*, 175:125–128, 2015.

[6] J.A. Feijo and N. Moreno. Imaging plant celss by two-photon exciation. *Protoplasma*, 223:1–32, 2004.

[7] A. Rapaport, J. Milliez, M. Bass, A. Cassanho, and H. Jenssen. Review of the properties of up-conversion phosphors for new emissive displays. *Journal of Display Technology*, 2:68–78, 2006.

[8] X. Mateos, R. Solé, Gavaldà Jna., M. Aguiló, F. Díaz, and J. Massons. Ultraviolet and visible emissions of Er^{3+} in $KY(WO_4)_2$ single crystals co-doped with Yb^{3+} ions. *Journal of Luminescence*, 115:131–137, 2005.

[9] A. Strohhofer, C. Polman. Absorption and emission spectroscopy in Er^{3+}-Yb^{3+} doped aluminum oxide waveguides. *Optical Materials*, 21:705–712, 2003.

[10] Y. Song, Y. Huang, L. Zhang, Y. Zheng, N Guoab, and H. You. Gd_2O_2S:Yb,Er submicrospheres with multicolor upconversion fluorescence. *RSC Advances*, 2:4777–4781, 2012.

[11] M. Inokuti and F. Hirayama. Influence of energy transfer by the exchange mechanism on donor luminescence. *Journal of Chemical Physics*, 43:1978–1989, 1965.

[12] M. Yokota and O. Tanimoto. Effects of diffusion on energy transfer by resonance. *Journal of the Physical Society of Japan*, 22:779–784, 1967.

[13] A. I. Burshtein. Hopping mechanism of energy transfer. *Journal of Experimental and Theoretical Physics*, 35:1695–1701, 1972.

[14] W. J. C. Grant. Role of rate equations in the thery of luminescent energy transfer. *Physical Review B*, 4:648–663, 1971.

[15] P. Villanueva-Delgado, K. W. Krämer, and R. Valiente. Simulating energy transfer and upconversion in β-$NaYF_4$:Yb^{3+},Tm^{3+}. *Journal of Physical Chemistry*, 119:23648–23657, 2015.

[16] F. Wang and X. Liu. Recent advances in the chemistry of lanthanide-doped upconversion. *Chemical Society Reviews*, 39:976–989, 2009.

[17] J. B. Bünzli and S.V. Eliseeva. *Basics of Lanthanide Photophysics*. Springer-Verlag Berlin Heidelberg, 2010.

[18] J. De Wild. *Photon upconversion for thin film solar cells*. PhD thesis, University of Utrecht, 2012.

[19] A. de Bettencourt-Dias. *Luminescence of Lanthanide Ions in Coordination Compounds and Nanomaterials*. John Wiley and Sons, 2014.

[20] D. W. Ball. *Physical Chemistry*. 2003.

[21] H. C. Aspinall. *Chemistry of the f-Block Elements*. Gordon and Breach Science publishers, 2001.

[22] P.S. Peijzel, A. Meijerink, R. T. Wegh, M.F. Reid, and G.W. Burdick. A complete $4f^n$ energy level diagram for all trivalent lanthanide ions. *Journal of Solid State Chemistry*, 178:448–453, 2005.

[23] S. P. Sinha. *Systematics and the Properties of the Lanthanides*. D. Reidel Publishing Company, Dordrecht, 1 edition, 1983.

[24] P. Peijzel. *Probing high energy levels of lanthanides ions*. PhD thesis, University of Utrecht, 2004.

[25] Y. Li, Z. Song, C. Li, R. Wan, J. Qiu, Z. Yang, Z. Yin, y. Yany, X. Wang, and Q. Wang. Efficient near-infrared to visible and ultraviolet upconversion in polycrystalline BiOCl:Er^{3+}/Yb^{3+} synthesized at low temperature. *Ceramics International*, 39:8911–8916, 2013.

[26] R. W.G. Wyckoff. *Crystal Structures*, volume 1. John Wiley and Sons: New York, 2 edition, 1963.

[27] F. Wang, X. Chen, D. Liu, B. Yang, and Y. Dai. Experimental and theoretical study of pure and doped crystals: Gd_2O_2S, Gd_2O_2S:Eu^{3+} and Gd_2O_2S:Tb^{3+}. *Journal of Molecular Structure*, 1020:153–159, 2012.

[28] F.T. Rabouw. *Before there was light*. PhD thesis, University of Utrecht, 2015.

[29] T. Van Wijngaarden. *Speectral conversion for solar cells using metal nanoparticles and lanthanide ions*. PhD thesis, University of Utrecht, 2010.

[30] L. Aarts. *Downconversion for solar with lanthanide ion couples*. PhD thesis, University of Utrecht, 2009.

[31] J. Haitjema. The influence of donor-to-donor migration on luminescence, 2015.

[32] F.T. Rabouw, S.A den Hartog, T. Senden, and A. Meijerink. Photonic effects on the Förster resonance energy transfer efficiency. *Nature communications*, 5, 2014.

[33] J. F. Suyver, J. Grimm, M.K. van Veen, D. Biner, K. W. Krämer, and H. U. Güdel. Upconversion spectroscopy and properties of $NaYF_4$ doped with Er^{3+}, Tm^{3+} and/or Yb^{3+}. *Journal of Luminescence*, 117:1–12, 2006.

Appendices

A Convergence

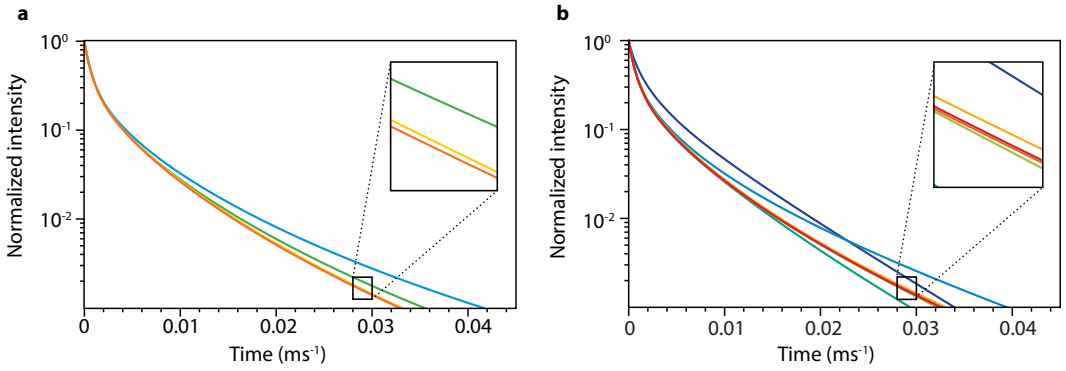

Figure 23: Convergence of the output data from simulations for a Gd_2O_2:Yb^{3+}(10%)Er^{3+}(2%) crystal system with a radiative rate for the donors of 3.45 ms^{-1} and migration and energy transfer rates of 3.7 $ms^{-1}nm^6$. Monte Carlo simulations as described in section 2.4.3 were used. **a.** Decay curves of donor emission for different box sizes: 5 (blue), 7 (green), 10 (orange), 15 (red). A minimum of 150 crystals and 20000 donors was set. **b.** Decay curves of donor emission for a crystal with boxsize 10, using different numbers of generated crystals: 1 (darkblue), 5 (blue), 10 (green), 100 (green-yellow), 500 (yellow), 1000 (orange), 2000 (red). The system converges at a box size of 10 and for a simulated number of crystals of 2000.